Monthly Notices
of the
ROYAL ASTRONOMICAL SOCIETY

MNRAS **445,** 3239–3262 (2014) doi:10.1093/mnras/stu1885

He-accreting white dwarfs: accretion regimes and final outcomes

L. Piersanti,[1,2]★ A. Tornambé[3] and L. R. Yungelson[4]

[1]*INAF-Osservatorio Astronomico di Collurania Teramo via Mentore Maggini, snc, I-64100 Teramo, Italy*
[2]*INFN-sezione di Napoli, I-80126 Napoli, Italy*
[3]*INAF-Osservatorio Astronomico di di Roma via di Frascati, 33, I-00040 Monte Porzio Catone, Italy*
[4]*Institute of Astronomy, Pyatnitskaya 48, 119017 Moscow, Russia*

Accepted 2014 September 9. Received 2014 September 5; in original form 2014 May 6

ABSTRACT

The behaviour of carbon-oxygen (CO) white dwarfs (WDs) subject to direct helium accretion is extensively studied. We aim to analyse the thermal response of an accreting WD to mass deposition at different timescales. The analysis has been performed for initial WD masses and accretion rates in the range 0.60–1.02 $M_\odot$ and 10^{-9}–10^{-5} $M_\odot$ yr^{-1}, respectively. Thermal regimes in the parameter space M_{WD}–$\dot{M}_{He}$ leading to formation of red-giant-like structures, steady burning of He, and mild, strong and dynamical flashes have been identified and the transition between these regimes has been studied in detail. In particular, the physical properties of WDs experiencing the He-flash accretion regime have been investigated to determine the mass retention efficiency as a function of the accretor total mass and accretion rate. We also discuss to what extent the building up of a He-rich layer via H burning could be described according to the behaviour of models accreting He-rich matter directly. Polynomial fits to the obtained results are provided for use in binary population synthesis computations. Several applications for close binary systems with He-rich donors and CO WD accretors are considered and the relevance of the results for interpreting He novae is discussed.

Key words: accretion, accretion discs – binaries: general – supernovae: general – white dwarfs.

1 INTRODUCTION

Accretion of helium onto carbon-oxygen (CO) white dwarfs (WDs) plays an important role in several astrophysical processes. Most significantly, it may have relevance to the problem of Type Ia supernova (SN Ia) progenitors. Among the hypothetical evolutionary paths to SNe Ia are semidetached close binary stars in which CO WDs grow in mass up to the Chandrasekhar mass limit (M_{Ch}) by accretion of matter directly from non-degenerate or degenerate helium-rich companions (e.g. Tutukov & Yungelson 1996; Yoon & Langer 2003; Solheim & Yungelson 2005; Wang et al. 2009), as well as explosions of sub-Chandrasekhar mass CO WDs via the edge-lit or double-detonation mechanism, in which detonation in the He-layer at the surface of an accreting WD triggers detonation of the CO accretor via shock waves that compress the latter (e.g. Nomoto 1980, 1982b; Livne 1990; Livne & Glasner 1991; Limongi & Tornambè 1991; Woosley & Weaver 1994; Livne & Arnett 1995; García-Senz, Bravo & Woosley 1999; Fink, Hillebrandt & Röpke 2007; Sim et al. 2010; Fink et al. 2010; Woosley & Kasen 2011; Schwab et al. 2012; Townsley, Moore & Bildsten 2012; Moll & Woosley 2013; Moore, Townsley & Bildsten 2013; Shen & Bildsten 2014).

Recent modification of the classical double-degenerate scenario (Iben & Tutukov 1984; Webbink 1984) envisions 'violent' or 'prompt' merger so that detonation is initiated at the interface of two merging WDs in a C-O or He-C-O mixture and determines the final complete burning of both WDs (e.g. Pakmor et al. 2010, 2011, 2012, 2013; Kromer et al. 2013; Moll et al. 2014). It is worth noting that some authors questioned whether carbon detonation is really prompt (e.g. Raskin et al. 2012). Moreover it has been shown that the location of the initial explosion does depend on the numerical resolution as well as on the initial configuration adopted in the computations (Dan et al. 2012, 2014). Double-detonation and violent merger scenarios are currently considered as alternative or complementary to the classical single-degenerate and double-degenerate scenarios for SNe Ia. For a review of the SN Ia progenitors and the observational constraints to theoretical models see, e.g. Hillebrandt et al. (2013), Höflich et al. (2013), Maoz, Mannucci & Nelemans (2014) and Postnov & Yungelson (2014), while for recent results of binary population synthesis (BPS) for SNe Ia from different channels see Ruiter, Belczynski & Fryer (2009), Wang et al. (2009), Mennekens et al. (2010), Ruiter et al. (2011), Toonen, Nelemans & Portegies Zwart (2012), Nelemans,

★E-mail: piersanti@oa-teramo.inaf.it

Toonen & Bours (2013), Ruiter et al. (2013) and Wang, Justham & Han (2013).

For the double-detonation scenario, the onset of the initial He detonation depends on the accretion rate and the mass of He retained at the WD surface.[1] For both scenarios the percentage of the He-rich matter transferred from the donor and effectively retained by the accreting WD and nuclearly processed into a C-O-rich mixture up to either the He detonation or the merger may be important since simulations show that physical conditions adequate to reproduce normal SNe Ia are more favourable in massive accretors – $M_{\rm WD} \gtrsim 0.8$ M$_\odot$ for double detonation (Livne & Glasner 1991; Fink et al. 2010; Kromer et al. 2010; Piro, Thompson & Kochanek 2014) and $M_{\rm WD} \gtrsim 0.9$ M$_\odot$ for violent mergers (Kromer et al. 2013; Pakmor et al. 2013). This means that the transfer of He-rich matter on to a newborn WD and its conversion into C and O may be necessary, as CO WDs typically form with lower masses.

In the classical single-degenerate scenario for Chandrasekhar mass SNe Ia, the retention efficiency of He is a crucial parameter, since the most important physical process involved is the nuclear burning of H into He and then into a C-O-Ne mixture (see e.g. Bours, Toonen & Nelemans 2013, for a recent discussion). Retention efficiency of helium and He-burning regimes are, for instance, also important for formation and evolution of AM CVn stars (Nelemans et al. 2001), the origin of faint and fast transients possibly associated with single He-layer detonation at the surface of accreting WDs, like the still hypothetical SNe .Ia (see e.g. Bildsten et al. 2007; Shen et al. 2010; Waldman et al. 2011; Woosley & Kasen 2011; Kasliwal 2012; Raskin et al. 2012; Sim et al. 2012; Shen & Bildsten 2014) and, possibly, some subluminous SNe Ia (Wang et al. 2013). Other problems include, e.g., the interpretation of events suggested to be helium novae (Ashok & Banerjee 2003; Rosenbush 2008).

The large majority of studies devoted to the thermal response of CO WDs accreting He-rich matter, have focused on defining physical conditions for the onset of either a very strong He flash or a He detonation (Sugimoto & Fujimoto 1978; Nomoto, Nariai & Sugimoto 1979; Nariai, Nomoto & Sugimoto 1980; Taam 1980a,b; Fujimoto & Sugimoto 1982; Nomoto 1982a,b; Woosley, Taam & Weaver 1986; Nomoto & Hashimoto 1987; Iben & Tutukov 1991; Limongi & Tornambè 1991; Woosley & Weaver 1994; Piersanti, Cassisi & Tornambé 2001; Bildsten et al. 2006; Shen & Bildsten 2007, 2009; Woosley & Kasen 2011). As a result, various accretion regimes have been roughly defined, depending both on the accretion rate and on the CO WD mass. In particular, Nomoto (1982a) suggested that for a high value of the accretion rate $\dot{M}$, but still below the Eddington limit, an extended He-rich layer is piled up and the WD expands to red giant (RG) dimensions. The minimum value of $\dot{M}$ for this is defined by the rate at which He burns into CO-rich matter at the base of the He envelope. Based on computations of massive pure-He stars by Uus (1970), Nomoto derived an analytical formula for such a limiting value:

$$\left(\frac{{\rm d}M}{{\rm d}t}\right)_{\rm RHe} = 7.2 \times 10^{-6}\,(M_{\rm CO} - 0.60) \qquad ({\rm in\ M_\odot\ yr^{-1}}), \qquad (1)$$

where $M_{\rm CO}$ is the mass of the CO core in M$_\odot$, varying in the range 0.75–1.38 M$_\odot$. For $\dot{M}$ less than $\sim 10^{-6}$ M$_\odot$ yr^{-1}, but larger than $\sim 10^{-7}$ M$_\odot$ yr^{-1}, He burning is stable and the CO core increases in mass steadily (Iben & Tutukov 1989). For lower values of the accretion rate, but larger than $\sim 3 \times 10^{-8}$ M$_\odot$ yr^{-1}, He burning proceeds through recurrent flashes, whose strength increases with decreasing $\dot{M}$, for a fixed mass of the CO core. In this case the He flashes are too weak to develop any dynamical effects, even if the large energy release can trigger the expansion of the accreting structure and, hence, the interaction with its binary companion (Taam 1980a; Fujimoto & Sugimoto 1982). Finally, for $\dot{M} \leq 3 \times 10^{-8}$ M$_\odot$ yr^{-1} a dynamical He flash occurs when a critical amount of He-rich matter has been accreted. Woosley & Kasen (2011) investigated in great detail the physical properties of He-accreting WDs at low accretion rates and defined very accurately the transition from nova-like He flashes to He detonation (see their fig. 19). They demonstrated that the He layer above the CO core could detonate only if the density at the ignition point is larger than a critical value, around 10^6 g cm^{-3}.

Kato & Hachisu (2004, hereafter KH04) calculated the retention efficiency $\eta_{\rm acc}$ of a He-accreting WD for CO cores in the range 0.6–1.3 M$_\odot$ and $3 \times 10^{-8} \leq \dot{M} \leq 1.5 \times 10^{-6}$ M$_\odot$ yr^{-1}. $\eta_{\rm acc}$ is defined as the ratio of the mass effectively accumulated on the CO core after one full He-flash-driven cycle and the amount of matter transferred from the donor during the same cycle. The computations by KH04 were based on the optically thick wind theory, which presumably describes the continuum-radiation-driven wind operating very deeply inside the photosphere (Kato & Hachisu 1994). Even though huge efforts have been applied to investigate the thermal response of CO WDs accreting He-rich matter, an overall picture is still missing. In particular, in the regime characterized by recurrent He flashes the possibility that accreting objects could overfill their Roche lobe has not been explored so far, despite this issue being of paramount importance in determining the long-term evolution of binaries harbouring He donors. The present work aims at a systematic analysis of the parameter space $M_{\rm WD}$–$\dot{M}$, considering fully evolutionary models of CO WDs with initial mass in the range 0.6–1.05 M$_\odot$[2] and accretion rates 10^{-9}–10^{-5} M$_\odot$ yr^{-1}. Based on our results, we intend to define the limits of different accretion regimes and the possible outcomes of the accretion process. Moreover, at variance with previous studies, we investigate the effects of the previous evolution, namely of the accretion history, on the actual thermal response of accreting WDs.

In Section 2 we describe our evolutionary code and the input physics. We also present the main properties of the initial CO WD models. In Section 3 we present our results and define various accretion regimes. In Section 4 we discuss under what conditions central C ignition could occur in a Chandrasekhar-mass WD, thus triggering an explosion. Section 5 is devoted to the accumulation efficiency in models directly accreting He-rich matter and as a by-product of H burning in H-accreting WDs. In Section 6 we discuss the formation of He-rich donors in close binaries and we analyse the applications of our results to several types of systems in which stable accretion of pure He onto a CO WD may occur. Our final considerations are reported in Section 7. Interpolation formulae to the data reported in this work are provided in Appendix. Detailed tables of data presented in Section 3 are provided in the Additional Supporting material available in the online version of this paper.

[1] We do not consider here He detonation initiated by instability in the accretion flow (Guillochon et al. 2010).

[2] 1.02 M$_\odot$ is the maximum mass of the newborn CO core at the beginning of the Thermally Pulsing Asymptotic Giant Branch (TP-AGB) phase in our evolutionary code. If the core exceeds this limit, C burning will be ignited at the centre or off-centre, depending on the total mass of the core. By assuming that during the AGB phase the CO core almost does not grow in mass, 1.05 M$_\odot$ represents the maximum mass for a CO WD.

Table 1. Physical properties of the initial CO WDs (*cool models*) and after the first mass transfer episode (*heated models*). We list the total mass of the model ($M_{\rm tot}$), the mass fraction abundance ratio of carbon over oxygen at the centre (C/O), the mass extension of the He-deprived core ($M_{\rm CO}$), the mass extension of the more external layer where the helium abundance by mass fraction is larger than 0.05 ($\Delta M_{\rm He}$), the temperature ($T_{\rm c}$ in kelvins) and the density ($\rho_{\rm c}$ in g cm^{-3}) at the centre, the surface luminosity (L), the effective temperature ($T_{\rm eff}$ in kelvins) and the surface radius (R). For more details, see the text.

	Cool models					Heated models				
Label	M060	M070	M081	M092	M102	M060	M070	M081	M092	M102
$M_{\rm tot}$ (in $M_\odot$)	0.600 00	0.700 00	0.808 33	0.919 62	1.020 61	0.596 78	0.701 85	0.810 33	0.918 97	1.020 48
C/O	0.3839	0.4308	0.5396	0.5371	0.4870	0.3839	0.4308	0.5396	0.5371	0.4870
$M_{\rm CO}$ (in $M_\odot$)	0.5158	0.6580	0.7921	0.9114	1.0157	0.5173	0.6580	0.7921	0.9116	1.0158
$\Delta M_{\rm He}$ (in 10^{-2} $M_\odot$)	3.37	1.40	0.73	0.39	0.18	1.62	0.67	0.30	0.13	0.06
$\log(T_{\rm c})$	7.8647	7.8644	7.8759	7.9915	8.0798	7.8318	7.8495	7.8593	7.9012	7.9528
$\log(\rho_{\rm c})$	6.4981	6.7518	7.0219	7.2792	7.5403	6.4552	6.7387	7.0187	7.2995	7.5779
$\log(L/L_\odot)$	0.5358	0.5637	0.4881	1.3760	2.7042	3.3358	3.7567	4.0224	4.2488	4.4‘87
$\log(T_{\rm eff})$	4.7996	4.8424	4.8606	5.0989	5.4154	5.2821	5.4382	5.5655	5.6850	5.7789
$\log(R/R_\odot)$	−1.8083	−1.8799	−1.9542	−1.9868	−1.9557	−1.3745	−1.4752	−1.5969	−1.7235	−1.8254

2 INPUT PHYSICS AND NUMERICAL METHODS

All the models presented in this study have been computed with an updated version of the F.RA.N.E.C code, the original version being described in Chieffi & Straniero (1989). The set-up of the code is the same as in Piersanti, Straniero & Cristallo (2007); in particular, we consider solar chemical composition models adopting the solar mixture GS98 derived in Piersanti et al. (2007). Tables of radiative opacities for temperatures lower than 5×10^8 K have been derived through the web facility provided by the OPAL group (http://opalopacity.llnl.gov/new.html, see Iglesias & Rogers 1996), while at higher temperatures we adopt the tables derived from the Los Alamos Opacity library (Huebner et al. 1977). The contribution of electron conduction to the total opacity has been included according to the prescription by Potekhin et al. (1999). We adopt the equation of state computed by Straniero (1988) and successive upgrades (Prada Moroni & Straniero 2002). Matter is accreted by assuming that it has the same specific entropy as the external layers of the CO WD; this is equivalent to the assumption that the energy excess is radiated away (Piersanti et al. 2000, and references therein). We fix the chemical composition of the accreted matter to $X=0$, $Y=0.98$, $Z=0.02$, where X, Y and Z are the mass fraction abundance of hydrogen, helium and metals, respectively. Since the He donor has formed via nuclear burning of H-rich matter, we assume that all the initial CNO elements have been converted into ^{14}N (i.e. $Y^i_{^{12}\rm C} + Y^i_{^{13}\rm C} + Y^i_{^{14}\rm N} + Y^i_{^{15}\rm N} + Y^i_{^{16}\rm O} + Y^i_{^{17}\rm O} + Y^i_{^{18}\rm O} = Y^f_{^{14}\rm N}$ where $Y_{\rm j}$ is the abundance by number of the j isotope and the subscripts i and f refer to the initial main-sequence star and the final He-donor star, respectively). For all the elements heavier than oxygen we assume a scaled-solar chemical composition.

The adopted nuclear network includes elements from H to Fe, linked by α-, p- and n-capture reactions as well as $\beta^{\pm}$ decays. We do not consider the NCO chain (^{14}N(e$^-$, ν)^{14}C(α, γ)^{18}O) because it has been demonstrated that its contribution to the energy budget does not have a sizable effect on the physical properties of accreting WDs (Piersanti et al. 2001).

The convective mixing is modelled by means of the time-dependent algorithm introduced by Sparks & Endal (1980) and successively modified by Straniero, Gallino & Cristallo (2006) (for a recent review see also Straniero, Cristallo & Piersanti 2014). In this case the degree of convective mixing between two points inside the convective zone depends on the corresponding turnover timescale.

To obtain the initial CO WD models, we evolved intermediate mass stars from the pre-main sequence to the cooling sequence, by assuming that they are components of interacting binary systems. For models M060 and M070, we assumed that their progenitors experienced a common envelope episode during the RG phase, while for progenitors of models M081, M092 and M102, we assumed a Roche lobe overflow (RLOF) in the hydrogen-shell burning stage while they possessed radiative envelopes. Some physical properties of the initial WD models are summarized in Table 1 (*cool models*).

The deposition onto the *cool models* of He-rich matter at a relatively high rate (say, $\dot{M}$ >5–10 $\times$ 10^{-8} $M_\odot$ yr^{-1}) determines the heating of the physical base of the He-rich layer, because the adopted initial models are compact and cool (their luminosity is definitively lower than that of a post-AGB star of the same mass). Hence, the compressional heating timescale at the surface of the accretor is definitively shorter than the inward thermal diffusion timescale. As a consequence the temperature at the base of the He-rich layer increases and He burning is ignited when the local temperature attains $\sim 10^8$ K. However, due to the partial degeneracy at the ignition point,[3] a thermonuclear runaway occurs, even if the resulting flash does not become dynamical. The accreting WD reacts to the injection of a huge amount of nuclear energy by expanding to giant dimensions ($R_{\rm WD} > 100\,R_\odot$). When considering that these objects are components of binary systems, it turns out that they have to experience a RLOF, losing part of the matter previously accreted.

We simulated this first flash episode by adopting $\dot{M} = 10^{-7}$ $M_\odot$ yr^{-1}. Moreover, for all the considered models we fix the radius of the Roche lobe to $R_{\rm Roche} = 10\,R_\odot$. It is worth noticing that, even if such an assumption is completely arbitrary, the physical properties of the final structure do not depend on the exact value of $R_{\rm Roche}$, since the expansion to giant dimensions occurs on a very short timescale, smaller than the nuclear timescale of the He-burning shell[4] and the inward thermal diffusion timescale.

We find that during this first mass transfer episode, the amount of material effectively deposited onto the WDs is practically zero

[3] We define the ignition point as the mass coordinate where the nuclear production via 3α reactions is at a maximum at the epoch when the energy per unit of time delivered by He burning is 100 times the surface luminosity. This implies that at the ignition point $\varepsilon_{\rm nuc} > \varepsilon_\nu$.

[4] The He-burning shell is defined as the mass coordinate where the energy production via 3α reactions is at a maximum.

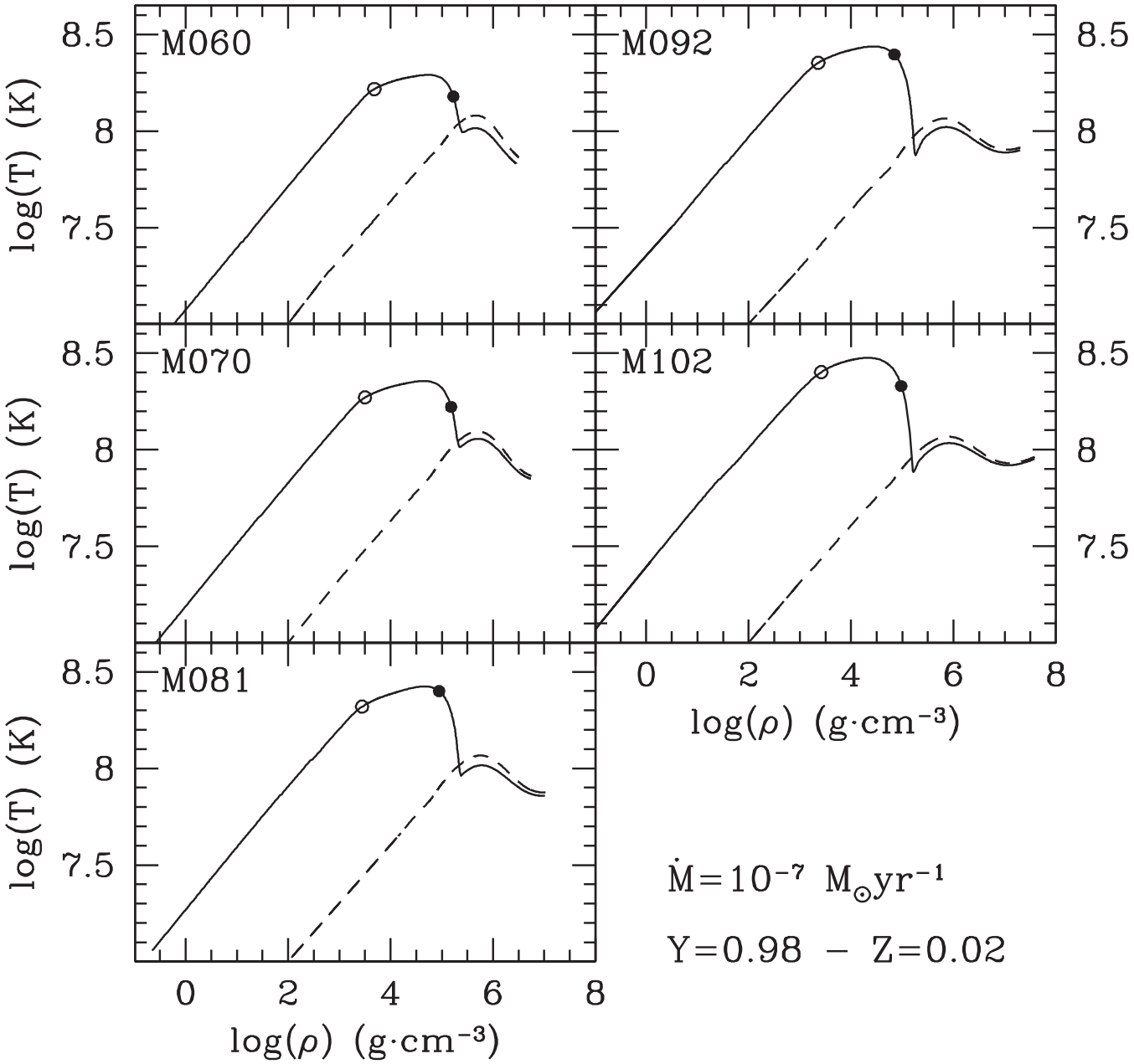

Figure 1. Profiles in the ρ–T plane for the *cool* (dashed lines) and *heated models* (solid lines). Each panel refers to one CO WD as labelled. In the profiles of *heated models* we mark with a filled circle the He/CO interface and with an open circle the He-burning shell.

(in some cases the pre-existing He-rich zone is also eroded). The only effect of the first He flash is just to modify the physical properties of the He-rich layer (mainly temperature and density profiles), so that the He shell attains the conditions for steady burning. This is clearly depicted in Fig. 1 where we show, for each considered model, the profile in the ρ–T plane for WDs at the beginning of the first mass transfer episode (dashed lines) and after the RLOF episode, when a WD has attained its maximum effective temperature at the beginning of the cooling sequence (solid lines). Henceforth, we address these models with a modified thermal structure of the envelope as *heated models*. In Table 1, we report also some relevant physical quantities for each model after the first He-flash episode. The CO core is defined as the portion of the star where the helium abundance is lower than 10^{-20} by mass fraction, while the He-burning shell is defined as the mass coordinate where He burning is a maximum. The physical and chemical conditions for $\varepsilon_{\rm nuc}$ to be a maximum are far from the He/CO interface, but close to the mass coordinate where He abundance is ∼0.05 by mass fraction. The He-burning shell does not correspond to the maximum temperature because, after the RLOF episode, it moves outward, where the temperature is lower, while the newly synthesized CO layer contracts and heats up.

3 ACCRETION REGIMES

We accrete He-rich matter directly onto *heated* CO WDs (see previous section) by adopting values for the accretion rate in the range $10^{-9} \leq \dot{M} \leq 10^{-5}$ M$_\odot$ yr^{-1}. The starting point for all the computations is defined along the high luminosity branch, during the blueward evolution of the post-first-flash steady-state structure.

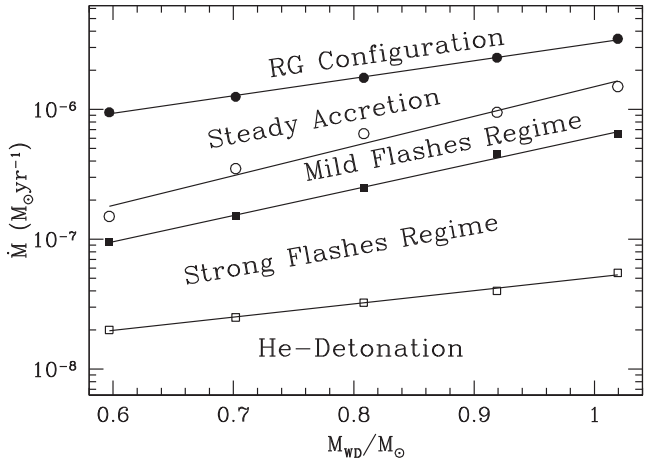

Figure 2. Possible accretion regimes as a function of the WD initial mass and accretion rate. Solid lines represent the transition between different accretion regimes as obtained by linearly interpolating the results of our computations (open and filled symbols). Interpolation formulae are presented in Appendix A1.

Our results are summarized in Fig. 2, where we show the possible accretion regimes as a function of the WD initial mass and accretion rate. The lines marking the transition from one accretion regime to another have been obtained by considering the thermal response of *heated models* to the mass transfer. For example, for the model M081 we fix the transition from the steady accretion to the mild flashes at $\dot{M} = 6.5 \times 10^{-7}$ $M_\odot$ yr^{-1}, since for $\dot{M} = 7 \times 10^{-7}$ $M_\odot$ yr^{-1} the model is in a steady state while for $\dot{M} = 6 \times 10^{-7}$ $M_\odot$ yr^{-1} it experiences recurrent mild flashes (see below for the definitions of different regimes).

3.1 Dynamical He-flash regime

At low accretion rates, the physical base of the He-rich mantle cools down and becomes degenerate. Later on, due to the continuous deposition of matter, it heats up and He burning is ignited. Owing to the degeneracy at the ignition point, the nuclear energy delivered by the 3α reactions is stored locally producing the increase of temperature and causing a thermonuclear runaway (He flash). However, the degeneracy level at the ignition point is only a necessary condition to trigger a dynamical burning event. Indeed, the He flash triggers the formation of a convective shell, which extends outward as the temperature increases at the base of the He-rich zone. The convective shell injects fresh He into the burning zone fuelling the thermonuclear runaway and, hence, the continuous increase of the local temperature. As a matter of fact, if the mass of the He-rich layer (and, hence, the total He abundance by mass) is too small, the propelling effect of convective mixing rapidly exhausts, the flash quenches and the accreting WD expands (for a more detailed discussion see Section 3.2).

For accretion rates lower than $\sim 5 \times 10^{-8}$ $M_\odot$ yr^{-1} the whole structure becomes isothermal very rapidly, independently of the initial temperature profile, since the inward thermal diffusion timescale is very small compared to the accretion timescale ($\tau_{\rm diff} \sim 10^5$ yr, while $\tau_{\rm acc} > 10^7$ yr). This also implies that the energy delivered by the mass deposited on the surface of the WD cannot produce a local increase of temperature. As a consequence, the nature of the final He flash (explosion or not) depends only on the interplay between the neutrino cooling of the physical base of the He shell and the heating driven by the compression of the whole structure. Since the latter quantity depends on the mass growth timescale, it turns out that, for a fixed total mass of the initial WD, the nature of the final He flash depends only on the accretion rate: if it is smaller than a critical value $\dot{M}({\rm He})_{\rm expl}$, the He shell becomes strongly degenerate and the resulting flash turns into an explosion.

In our computations, following Bildsten et al. (2007) and Shen & Bildsten (2009), we check the onset of a dynamical flash by comparing $\tau_{\rm heat}$, the heating timescale due to release of nuclear energy, and $\tau_{\rm dyn}$, the dynamical timescale, at the He-burning shell. If $\tau_{\rm heat}$ becomes smaller than $\tau_{\rm dyn}$, the He-rich zone above the He-burning shell cannot readjust to a new equilibrium configuration and, hence, the evolution decouples, driving to the formation at the interface of an overpressure, which triggers the explosion. These two characteristic timescales have been computed according to the following relations:

$$\tau_{\rm heat} = \frac{C_P T}{\varepsilon_{\rm nuc}},$$
$$\tau_{\rm dyn} = \frac{H_P}{v_{\rm sound}}, \qquad (2)$$

where $C_{\rm P}$ is the specific heat at constant pressure, T the temperature, $\varepsilon_{\rm nuc}$ the rate of energy production via nuclear burning, $H_{\rm P}$ the pressure scale height and $v_{\rm sound}$ the local sound velocity.

Our results are summarized in Table 2, where we report, as a function of the accretion rate, the total final mass ($M_{\rm fin}$), the accreted mass ($M_{\rm acc}$) and the corresponding accretion time ($T_{\rm acc}$), the mass coordinate of the point where the He flash is ignited ($M_{\rm ig}$) and the value of temperature ($T_{\rm ig}$) and density ($\rho_{\rm ig}$) at the ignition point for some representative computed models. In the last column we report $\Delta M^{\rm pk}_{\rm He}$, defined as the total mass of the layer where He abundance is larger than 0.01 by mass fraction. Note that the latter

Table 2. Models experiencing dynamical He flashes. For each model we list as a function of the accretion rate ($\dot{M}$ in 10^{-9} $M_\odot$ yr^{-1}), the final mass ($M_{\rm fin}$ in $M_\odot$), the accreted mass ($M_{\rm acc}$ in $M_\odot$), the accretion time ($T_{\rm acc}$ in 10^6 yr), the mass coordinate where He burning is ignited ($M_{\rm ig}$ in $M_\odot$), the temperature ($T_{\rm ig}$ in 10^7 K) and density ($\rho_{\rm ig}$ in 10^6 g cm^{-3}) when He burning is ignited. The last column gives the mass of the zone where helium abundance by mass fraction is larger than 0.01 ($\Delta M^{\rm pk}_{\rm He}$ in $M_\odot$). A more detailed table with small increments in $\dot{M}$ is available online.

$\dot{M}$	$M_{\rm fin}$	$M_{\rm acc}$	$T_{\rm acc}$	$M_{\rm ig}$	$T_{\rm ig}$	$\rho_{\rm ig}$	$\Delta M^{\rm pk}_{\rm He}$
			M060				
1	1.255	0.658	658.4	0.587	5.246	72.061	0.737
5	1.092	0.495	99.1	0.601	7.579	13.452	0.571
15	0.971	0.374	24.9	0.608	8.619	4.995	0.448
			M070				
1	1.277	0.575	698.0	0.698	5.124	75.664	0.616
5	1.123	0.421	84.2	0.715	7.648	12.802	0.457
20	0.913	0.211	10.6	0.735	9.442	1.839	0.252
			M081				
1.5	1.263	0.453	301.7	0.818	6.071	45.067	0.461
6	1.144	0.333	55.6	0.825	7.851	10.913	0.342
25	0.912	0.102	4.1	0.826	9.947	0.929	0.111
			M092				
1.5	1.301	0.383	255.2	0.918	5,799	59.903	0.392
7	1.180	0.262	37.4	0.930	7,844	10.624	0.271
30	0.963	0.045	1.491	0.922	10.534	0,590	0.053
			M102				
1.5	1.318	0.299	199.7	1.019	5.883	92.234	0.305
8	1.204	0.185	23.1	1.028	8.075	8.791	0.190
50	1.039	0.020	0.4	1.021	11.148	0.427	0.025

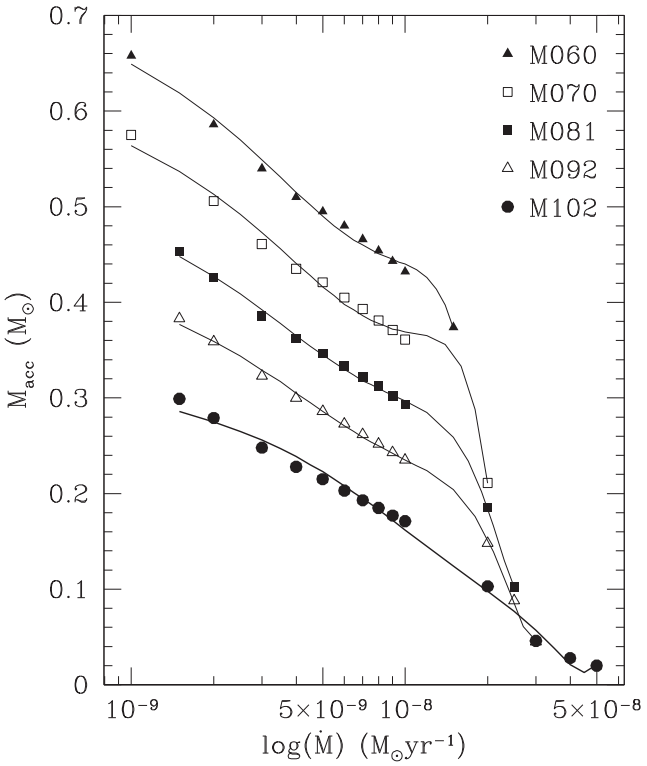

Figure 3. Accreted mass as a function of the accretion rate for models experiencing a dynamical He flash. Each set of symbols refers to a different initial model, as labelled in the figure. Solid lines represent polynomial fits to the data (see Appendix A2).

is slightly larger than the accreted mass since the initial WD models are capped by a He-rich layer, determined by the previous evolution, which is much smaller than the mass to be accreted for igniting a dynamical He flash (see Section 2). Polynomial fits of $M_{\rm acc}$ as a function of the accretion rate for all the models displayed in Fig. 3 are provided in Appendix A2. Where comparable, for $M_{\rm WD} = 0.6$–$1.0\ {\rm M}_\odot$, minimum accreted masses necessary for a dynamical He flash are in very good agreement, within a factor of less than 2, with the estimates obtained by Shen et al. (2010). As well, in agreement with the latter study we find that the ignition mass depends on $\dot{M}$. In Fig. 3 we present the accreted mass as a function of the accretion rate for each initial WD model. At variance with Nomoto (1982a) and in agreement with Shen et al. (2010), we find that the maximum value of the accretion rate still producing a dynamical He flash slightly depends on the WD mass (see Fig. 2). By interpolating the data reported in Table 2 we obtained (in $\rm M_\odot\ yr^{-1}$)[5]:

$$\log(\dot{M}({\rm He})_{\rm expl}) \approx (1.15 \pm 0.11)\frac{M_{\rm WD}}{\rm M_\odot} - (8.52 \pm 0.07). \quad (3)$$

To investigate the dependence of our results on the history of the accretion rate, we computed an additional set of models, by adopting as initial CO WD the M092 model and a time-dependent accretion rate, given by:

$$\dot{M} = (2.75 \times {\rm e}^{-t/\tau} + 0.15) \times 10^{-8}\ {\rm M_\odot\ yr^{-1}}, \quad (4)$$

[5] Equation (3) gives the *highest* value of $\dot{M}_{\rm He}$ for which in our computations He definitely detonates, while the limits shown in Fig. 2 and the corresponding formulae in Appendix A1 represent results of interpolation between models experiencing different burning regimes, because of the finite resolution of the adopted accretion rate grid.

Table 3. The same as Table 2, but for model M092 accreting He-rich matter at $\dot{M} = (2.75 \times {\rm e}^{-t/\tau} + 0.15) \times 10^{-8}\ {\rm M_\odot\ yr^{-1}}$, with different values of the characteristic timescale τ, as listed in the first column in 10^6 yr. See text for more details.

τ	$M_{\rm fin}$	$M_{\rm acc}$	$T_{\rm acc}$	$M_{\rm ig}$	$T_{\rm ig}$	$\rho_{\rm ig}$	$\Delta M^{\rm pk}_{\rm He}$
4	1.300	0.382	181.239	0.918	5.823	58.871	0.393
6	1.298	0.380	143.235	0.918	5.870	56.824	0.391
8	1.290	0.372	101.557	0.918	6.040	49.957	0.383
9	1.259	0.341	62.223	0.918	6.606	30.342	0.351
10	1.140	0.222	13.316	0.928	8.259	6.808	0.233
15	0.995	0.077	2.903	0.928	9.912	1.053	0.085
20	0.984	0.066	2.403	0.926	0.096	0.882	0.074

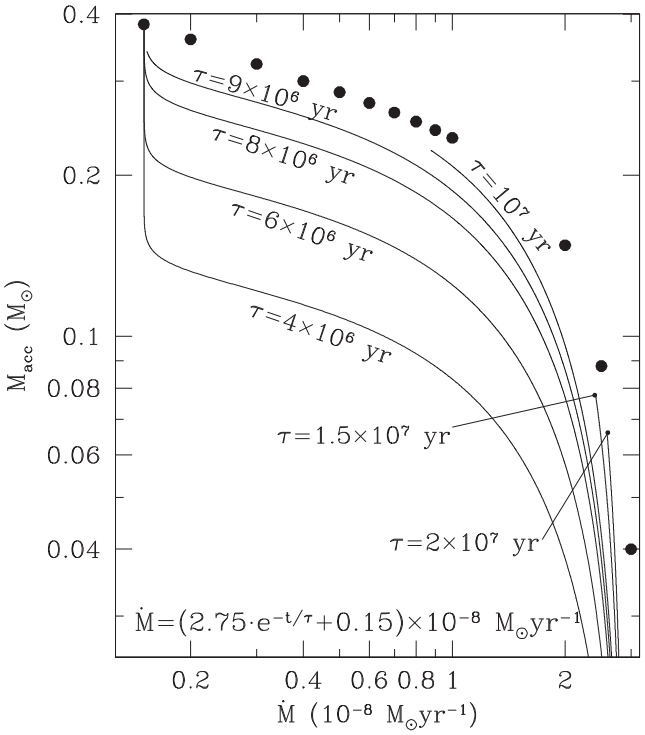

Figure 4. The same as Fig. 3, but for the M092 CO WD accreting He-rich matter with an exponentially decaying accretion rate, as reported in the figure. Different models have different decay timescales, as labelled. Large dots represent total accreted mass for models with constant accretion rate.

where τ is a characteristic timescale varying in the range 4–20 Myr. The results are summarized in Table 3, where we list the same quantities as in Table 2.

In Fig. 4, we plot the amount of accreted mass as a function of the accretion rate for the models listed in Table 3 and, for comparison, we also show the total accreted mass of models with constant accretion rate (filled dots). As can be noticed, the mass accreted before the onset of the dynamical He flash depends both on the accretion rate and on the accretion history. In particular, Fig. 4 reveals that the leading parameter determining $M_{\rm acc}$ is the actual value of $\dot{M}$ at the onset of the He flash, while the previous mass transfer process has a minor role, just reducing by less than 10 per cent the value of the accreted mass. In any case, if $\dot{M}$ decreases very rapidly, the accreting WD loses memory of the previous evolution and the evolution to the explosion occurs exactly as it would if $\dot{M}$ were kept constant from the very beginning and equal to its final value.

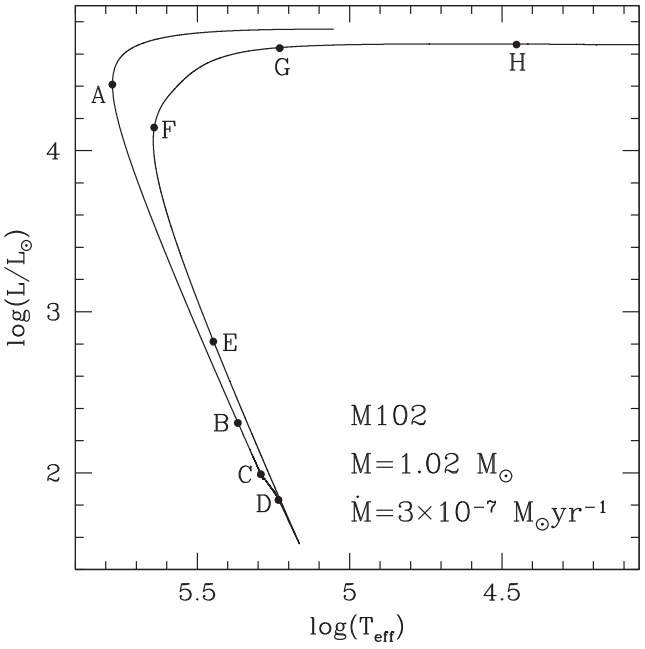

Figure 5. Evolution in the HR diagram of the M102 model accreting He-rich matter at $\dot{M} = 3 \times 10^{-7}$ M$_\odot$ yr^{-1}. The points along the track represent: A, the bluest point; B, minimum He-burning luminosity; C, start of flash-driven convection; D, maximum extension of the flash-driven convective shell; E, maximum He-burning luminosity; F, beginning of the flash-driven convective shell backtrack; G, die down of flash-driven convection and H, appearance of surface convection. For more details, see the text.

3.2 Strong flashes regime

For slightly larger values of the accretion rate, the He flash does not become dynamical, as the nuclear timescale at the base of the He-rich layer never approaches $\tau_{\rm dyn}$. However, the released energy is huge, so that an expansion to giant dimensions occurs. To illustrate the evolution of models experiencing this accretion regime, we show in Fig. 5 the evolution in the HR diagram of the model M102 accreting He-rich matter at 3×10^{-7} M$_\odot$ yr^{-1}. We mark by filled dots and letters some crucial moments during the evolution. In our analysis we follow the approach used by Piersanti et al. (2000) to discuss the evolution of H-accreting models (see also the references therein). The evolution is counterclockwise along the track and we start our discussion from point A in Fig. 5, the bluest point of the whole track. This point represents a bifurcation in the evolution of He-accreting models. At this stage the He-burning shell is very close to the surface and cool and, in addition, the mass of the He-rich zone has been reduced below a critical value at which release of nuclear energy exceeds release of gravothermal energy. Hence, the energy production via He burning rapidly decreases and the gravothermal energy becomes the main source of energy.[6] During the following evolution the model approaches the WD radius appropriate to its mass, while the He-burning luminosity continues to decrease and after $\Delta T_{\rm AB} \simeq 1555$ yr it attains its minimum ($L_{\rm He} = 2.19 \times 10^{33}$ erg s^{-1}) at point B.

During the following evolution, which lasts for $\Delta T_{\rm BC} \simeq 5476$ yr, due to the continuous deposition of matter, the physical base of the He shell begins to heat up and nuclear burning via 3α reactions gradually resumes. Note that, even if the degeneracy of the He-burning shell is not high, the local nuclear timescale is shorter than the timescale for the thermal response of the star to a structural change. As a consequence, He burning turns into a flash. Very soon, the flash triggers the formation of a convective shell (point C in Fig. 5), which rapidly increases in mass, attaining very soon the surface (point D). It is important to remark that also the inner border of the convective zone moves inward and this causes the He-burning shell to become more internal. In the model considered here, the convective unstable zone attains its maximum mass extension after $\Delta T_{\rm CD} \simeq 16.33$ yr. The onset of convection has two main effects: on one hand the nuclear energy delivered locally by He burning is transferred outward, thus limiting the thermonuclear runaway; on the other hand, convection dredges down fresh helium into the burning zone so that the thermonuclear runaway speeds up. When the evolutionary timescale becomes very short, the feeding of the He-burning shell by convection becomes inefficient and the structure reacts by evolving towards high luminosity. After $\Delta T_{\rm DE} \simeq 0.48$ d, it attains point E along the HR track, where the He-burning luminosity is at a maximum: $L_{\rm He} = 3.63 \times 10^{42}$ erg s^{-1}. The continuous expansion of the whole He-rich zone occurs at the expense of its thermal energy, so that He burning occurs at a progressively lower rate; hence, the flash-driven convection starts to recede very soon after $\Delta T_{\rm EF} \simeq 3.39$ d (point F in Fig. 5) and it definitively disappears at point G ($\Delta T_{\rm FG} \simeq 10.82$ yr).

The He flash drives the transition of the accreting model from a low state, corresponding to the cooling of the structure, to a high state, corresponding to the high luminosity branch. In fact, the He flash provides the thermal energy needed for quiescent He burning to set in, modifying the temperature and the density at the base of the He-rich layer. For the strong flashes regime, the amount of nuclear energy delivered during the flash largely exceeds the energy required for such a transition. This implies that the large thermal energy produced by He burning is initially locally stored and, later, redistributed along the whole zone above the He-burning shell. Under this condition the He-rich layer has a thermal content that is too large, which has to be dissipated before quiescent He burning can set in. Hence, the expansion towards the red part of the HR diagram is the natural consequence of the strong flash. Obviously, the lower the accretion rate, the stronger the resulting He flash and, hence, the larger the final radius attained by the accreting model. During the expansion along the high luminosity branch, surface convection sets in (point H) and it penetrates inward as the effective temperature decreases. The expansion from point G to H occurs in about $\Delta T_{\rm GH} \simeq 13.28$ yr. We forcibly halt the computation when the surface temperature becomes less than 11 300 K, since the adopted opacity tables are inadequate to describe models with lower $T_{\rm eff}$. Indeed, due to the overlap of the flash-driven convective shell and convective envelope, the surface abundance of heavy elements (mainly ^{12}C) increases well above the total metal content usually adopted in the computation of low-temperature opacity tables.

Considering that the accreting WD is a component of an interacting binary system, it turns out that during the expansion phase a fraction of the matter previously accreted can be lost by the WD, thus limiting the growth in mass of the CO core. This problem has been investigated in detail by KH04, who derived the amount of mass effectively retained by the accreting WD in the framework of the optically thick wind theory (Kato & Hachisu 1994). According to this approach, after the He flash, during the expansion to giant dimensions, wind mass loss starts when the photospheric temperature decreases to a critical value ($\log(T_{\rm ph}/K) \simeq 5.45$). During the redward evolution, the wind mass loss rate increases as the photospheric temperature decreases until the WD attains thermal

[6] The reasons for this are discussed in Iben (1982).

equilibrium and stops to expand, coming back blueward. The continuous loss of matter reduces the layer above the He-burning shell and, when the photospheric temperature of the star becomes larger than the critical value, it becomes negligible. The following evolution is driven by He burning, which reduces the mass of the He-rich layer, up to the bluest point in the HR diagram, when the burning dies and the structure becomes again supported by gravothermal energy. Kato & Hachisu (1994) claimed that the strong optically thick wind prevents the onset of a RLOF. Moreover, they suggested that, even if a RLOF could occur, a common envelope phase is avoided in any case, because the wind velocity is much larger than the orbital velocity of the two components in the binary system, so that the heating and the consequent acceleration of the lost matter are practically inefficient. However, as discussed in KH04, for CO WDs less massive than 0.8 $M_\odot$ the optically thick wind does not occur and all the matter is effectively deposited onto the WD, 'if the binary separation is large enough for the expanded envelope to reside in the Roche lobe.' Moreover, KH04 analyses the behaviour of CO WDs only for very large values of the accretion rate, not exploring the whole parameter space reported in our Fig. 2.

At variance with KH04, in the present work we do not assume that the optically thick wind operates and we compute the post-flash evolution of CO WDs experiencing strong flashes by assuming that a RLOF occurs. When the surface radius of the accreting WD becomes larger than the corresponding $R_{\rm Roche}$ we subtract mass by requiring that the star remains confined inside its lobe. When the WD definitively starts to contract, we allow the accretion to resume and we follow the evolution up to the bluest point of the loop in the HR diagram. Hence, the accumulation efficiency along the cycle is computed as:

$$\eta_{\rm acc} = 1 - \frac{\Delta M_{\rm L}}{\Delta M^1_{\rm tr} + \Delta M^2_{\rm tr}} \qquad (5)$$

where $\Delta M_{\rm L}$ is the mass lost during the RLOF, while $\Delta M^1_{\rm tr}$ and $\Delta M^2_{\rm tr}$ are the mass accreted onto the WD before and after the RLOF episode, respectively. In real binaries, the value of $R_{\rm Roche}$ is determined by the parameters of the system itself, i.e. the masses of primary and secondary components and the separation. For this reason, we computed some tests by fixing the initial WD mass (namely the M102 model) and varying the value of $R_{\rm Roche}$ in the range 1–45 $R_\odot$.[7] Our results show that the uncertainty in the estimated $\eta_{\rm acc}$ is smaller than 7–8 per cent. For this reason, we set $R_{\rm Roche} = 10$ $R_\odot$ in the computations of all the models experiencing strong flashes. The values of $\eta_{\rm acc}$ computed according to equation (5) are displayed in Fig. 6 as a function of the accretion rate for each CO WD model. Note that they refer to the first strong He flash experienced by all the *heated models* listed in Table 1. As can be noticed, as the accretion rate decreases, the accumulation efficiency reduces very rapidly. Indeed, on with lowering $\dot{M}$, the resulting He flash is stronger and, hence, a larger amount of mass has to be removed to dissipate the extra energy content of the whole He-rich layer. For the M102 model, the accumulation efficiency for $\dot{M}$ lower than 10^{-7} $M_\odot$ yr^{-1}, becomes negative; this means that during the RLOF episode the thin He-rich layer already existing at the bluest point in the HR diagram has been partially eroded. Polynomial fits of $\eta_{\rm acc}$ as a function of the accretion rate for all the models displayed in Fig. 6 are provided in Appendix A3.

[7] Note that the maximum considered value for $R_{\rm Roche}$ depends on the CO WD mass, because as already recalled, we stop the computation when the photospheric temperature becomes lower than 11300 K.

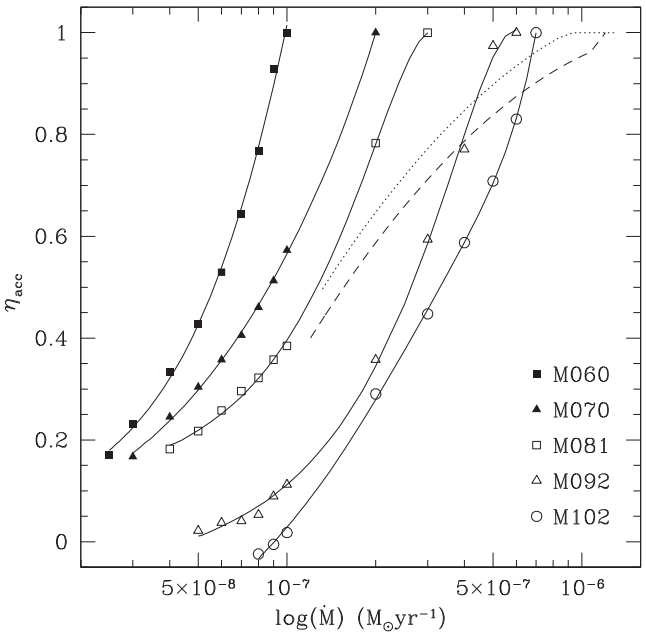

Figure 6. Accumulation efficiency $\eta_{\rm acc}$ as a function of the accretion rate for models of different initial mass as labelled inside the figure. Solid lines display polynomial fits to the data (see Appendix A3). The dotted and dashed lines represent the accumulation efficiency determined by KH04 for CO WDs with initial mass 0.9 and 1.0 $M_\odot$, respectively (their equations (4) and (5)).

In Table 4 we list, for each initial CO WD model, the accretion rate, the total mass at the bluest point along the loop in the HR diagram, the amount of mass transferred from the donor before and after the RLOF, the mass lost during the RLOF episode and the corresponding accumulation efficiency, as well as some other relevant physical quantities. By inspecting Table 4, it is evident that for each initial CO WD, the amount of matter accreted after the RLOF is negligible, even if it increases as the accretion rate increases. Moreover, Table 4 reveals that, for the computed models, the flash-driven convective shell extends all over the accreted layer and the most external zone of the He-rich mantle already existing at the epoch of the bluest point in the HR diagram loop. This implies that at the onset of the RLOF episode, the zone above the He-burning shell has been completely homogenized and, hence, it is depleted in helium and enriched in carbon, the resulting oxygen production being marginally efficient. In the last three columns of Table 4, we report the average chemical composition of the ejected matter. As can be noticed, for a fixed initial CO WD, the lower the accretion rate, the stronger the He flash and, thus, the more efficient the He consumption and the larger the carbon abundance. Moreover, the larger the initial CO WD, the lower the amount of matter accreted before the RLOF and, hence, the mass of the convective shell, so that, on average, the dilution of the He-burning ashes is lower and the resulting ^{12}C abundance in the ejecta becomes larger.

As shown in Table 4, for a fixed initial CO WD, $\Delta M^{\rm R}_{\rm He}$, the post-RLOF mass of the He-rich envelope above the He-burning shell $M^R_{\rm He}$, is largely independent of $\dot{M}$. This reflects that the location along the high luminosity branch, i.e. the effective temperature and, hence, the surface radius, depends on the mass of the He layer above the burning shell. Notwithstanding, Table 4 reveals that $\Delta M^{\rm R}_{\rm He}$ still slightly depends on the accretion rate: in initial low-mass CO WD models it is larger for higher $\dot{M}$, while in more massive ones it exhibits a maximum for intermediate values of $\dot{M}$.

Table 4. For each model listed in Table 1 experiencing strong flashes, we report as a function of the accretion rate ($\dot{M}$ in 10^{-8} $M_\odot$ yr^{-1}), the value of the total mass at the bluest point along the HR-diagram loop (M_{BP} in $M_\odot$), the masses transferred up to the onset and after the RLOF episode (ΔM_{tr}^1 and ΔM_{tr}^2, respectively, in $10^{-3}M_\odot$), the mass lost during the RLOF episode (ΔM_L in $10^{-3}M_\odot$), the accumulation efficiency (η_{acc}), the mass coordinate of the He-burning shell at the epoch of the maximum extension of the flash-driven convective shell (M_{He}^{CM} in $M_\odot$), the maximum extension of the flash-driven convective shell (ΔM_{He}^{CM} in $10^{-3}M_\odot$), the mass coordinate of the He-burning shell at the end of the RLOF (M_{He}^{R} in $M_\odot$) and the average chemical composition by mass fraction of the matter ejected during the RLOF.

$\dot{M}$	M_{BP}	ΔM_{tr}^1	ΔM_{tr}^2	ΔM_L	η_{acc}	M_{He}^{CM}	ΔM_{He}^{CM}	M_{He}^{R}	ΔM_{He}^{R}	^{4}He	^{12}C	^{16}O
						M060						
2.5	0.597 43	44.780	0.328	37.45	0.170	0.586 86	55.354	0.587 57	17.193	0.803	0.170	0.003
3.0	0.597 57	34.180	0.407	26.61	0.231	0.586 91	44.840	0.587 62	17.525	0.801	0.172	0.004
4.0	0.597 87	25.970	0.590	17.67	0.335	0.587 26	36.577	0.587 97	18.195	0.802	0.171	0.004
5.0	0.598 18	21.570	0.778	12.78	0.428	0.587 55	32.188	0.588 32	18.645	0.803	0.170	0.004
6.0	0.598 52	18.340	1.003	9.10	0.530	0.587 98	28.864	0.588 63	19.128	0.803	0.171	0.005
7.0	0.598 88	15.750	1.248	6.04	0.645	0.588 44	26.166	0.589 10	19.491	0.808	0.166	0.005
8.0	0.599 28	13.480	1.507	3.47	0.769	0.588 91	23.830	0.589 58	19.706	0.810	0.164	0.005
9.0	0.599 69	11.430	1.811	0.93	0.930	0.589 50	21.602	0.590 15	20.039	0.822	0.152	0.004
						M070						
3.0	0.702 03	31.220	0.089	26.07	0.167	0.697 79	35.457	0.698 69	8.495	0.758	0.212	0.003
4.0	0.702 09	22.090	0.125	16.77	0.245	0.697 84	26.341	0.698 73	8.686	0.752	0.219	0.004
5.0	0.702 16	18.460	0.163	12.96	0.304	0.697 91	22.703	0.698 76	8.892	0.752	0.220	0.004
6.0	0.702 22	16.110	0.202	10.48	0.358	0.697 98	20.353	0.698 83	9.026	0.753	0.219	0.004
7.0	0.702 29	14.320	0.240	8.65	0.406	0.698 03	18.578	0.698 92	9.037	0.755	0.217	0.005
8.0	0.702 36	12.880	0.282	7.10	0.461	0.698 10	17.123	0.698 92	9.215	0.756	0.216	0.005
9.0	0.702 43	11.580	0.323	5.75	0.517	0.698 18	15.899	0.699 00	9.253	0.765	0.208	0.004
10.0	0.702 50	10.610	0.366	4.68	0.573	0.698 29	14.801	0.699 08	9.336	0.763	0.209	0.005
						M081						
4.0	0.810 39	24.420	0.067	20.02	0.182	0.809 84	24.976	0.809 54	5.255	0.703	0.260	0.005
5.0	0.810 41	18.700	0.084	14.70	0.217	0.809 74	19.380	0.809 36	5.054	0.707	0.257	0.005
6.0	0.810 43	15.730	0.098	11.75	0.258	0.809 58	16.576	0.809 28	5.134	0.708	0.257	0.005
7.0	0.810 44	13.780	0.115	9.78	0.296	0.809 59	14.626	0.809 30	5.142	0.710	0.255	0.005
8.0	0.810 46	12.340	0.132	8.45	0.322	0.809 54	13.254	0.809 25	5.095	0.714	0.252	0.005
9.0	0.810 47	11.130	0.148	7.24	0.358	0.809 54	12.064	0.809 26	5.109	0.714	0.251	0.005
10.0	0.810 49	10.130	0.163	6.33	0.385	0.809 50	11.115	0.809 23	5.064	0.716	0.250	0.005
20.0	0.810 66	4.720	0.247	1.01	0.797	0.809 75	5.619	0.809 57	4.814	0.731	0.236	0.005
						M092						
5.0	0.918 99	15.590	0.015	15.27	0.022	0.918 28	16.304	0.917 42	1.885	0.586	0.352	0.019
6.0	0.918 99	12.680	0.017	12.22	0.038	0.918 27	13.402	0.917 72	1.727	0.603	0.344	0.012
7.0	0.918 99	10.910	0.020	10.48	0.041	0.918 27	11.633	0.917 58	1.836	0.606	0.343	0.013
8.0	0.919 00	9.620	0.023	9.13	0.053	0.918 28	10.335	0.917 64	1.845	0.607	0.342	0.013
9.0	0.919 00	8.730	0.023	7.97	0.089	0.918 28	9.449	0.918 05	1.703	0.609	0.342	0.013
10.0	0.919 00	7.980	0.027	7.10	0.113	0.918 29	8.689	0.918 07	1.810	0.611	0.340	0.013
20.0	0.919 03	4.220	0.052	2.73	0.359	0.918 32	4.915	0.918 73	1.781	0.621	0.334	0.013
30.0	0.919 06	2.640	0.088	1.10	0.596	0.918 38	3.311	0.918 62	1.980	0.643	0.315	0.011
40.0	0.919 10	1.920	0.104	0.45	0.776	0.918 44	2.559	0.918 78	1.791	0.676	0.286	0.008
50.0	0.919 14	1.450	0.114	0.03	0.983	0.918 56	1.996	0.918 93	1.630	0.809	0.161	0.002
						M102						
8.0	1.020 47	7.250	0.010	7.43	−0.023	1.020 19	7.540	1.019 55	0.740	0.545	0.355	0.020
9.0	1.020 47	6.460	0.000	6.49	−0.005	1.020 21	6.730	1.019 70	0.740	0.553	0.361	0.018
10.0	1.020 47	5.850	0.010	5.75	0.019	1.020 20	6.110	1.019 82	0.750	0.555	0.365	0.018
20.0	1.020 48	3.120	0.010	2.22	0.291	1.020 17	3.430	1.020 60	0.780	0.569	0.370	0.021
30.0	1.020 49	2.120	0.020	1.18	0.449	1.020 18	2.420	1.020 51	0.920	0.596	0.351	0.019
40.0	1.020 49	1.620	0.030	0.67	0.594	1.020 19	1.910	1.020 53	0.910	0.623	0.330	0.015
50.0	1.020 50	1.300	0.030	0.38	0.714	1.020 23	1.550	1.020 56	0.860	0.652	0.306	0.012
60.0	1.020 51	1.060	0.030	0.17	0.844	1.020 25	1.300	1.020 60	0.800	0.693	0.270	0.008

A further inspection of Table 4 reveals that at the end of the RLOF, the location of the He-burning shell becomes closer to the surface as $\dot{M}$ increases. Both these circumstances suggest that the strength of the He flash, which depends inversely on the accretion rate, plays a role in determining the actual value of the retention efficiency.

Encouraged by an anonymous referee to investigate in more detail such an issue, we computed several toy models, by fixing the initial CO WD (M102 model) and accretion rate ($\dot{M} = 3 \times 10^{-7}$ $M_\odot$ yr^{-1}), and by activating, after the ignition of He burning, an extra energy source in the layer where helium abundance is larger than 0.01 by mass fraction. This allows us to vary the strength of the flash, while ΔM_{tr}^1 as well as the ignition point remain unaltered. For simplicity, we parametrize the energy delivered by this fake source as $\varepsilon_{ES}(m) = \beta \varepsilon_{nuc}(m)$, where $\varepsilon_{nuc}(m)$ is the nuclear en-

Table 5. Selected physical properties of the test models computed by artificially varying the thermal content of the He-rich layer (see text for more details). For comparison we report also the standard case $\beta = 0.0$. $L_{\rm He}^{\rm Max}$ is the maximum luminosity of the He-burning shell and is expressed in 10^{42} erg s^{-1}. The other quantities are the same as in Table 4 and have the same units.

β	$L_{\rm He}^{\rm Max}$	$\Delta M_{\rm L}$	$\eta_{\rm acc}$	$\Delta M_{\rm He}^{\rm CM}$	$M_{\rm He}^{\rm R}$	$\Delta M_{\rm He}^{\rm R}$
			$\varepsilon_{\rm ES}({\rm m}) = \beta \times \varepsilon_{\rm nuc}({\rm m})$			
0.0	4.223	0.117	0.453	0.242	1.020 53	0.91
−0.5	2.559	0.075	0.648	0.237	1.020 91	0.96
0.2	4.609	0.124	0.423	0.244	1.020 37	1.00
0.5	5.022	0.130	0.393	0.245	1.020 29	1.02
			No convective mixing			
0.0	0.628	0.019	0.913	0.253	1.021 60	0.83
			Altered chemical composition			
–	9.282	0.158	0.251	0.242	1.020 27	0.76

ergy produced at the mass coordinate m and β a free parameter. A negative value for β means that energy is subtracted from the He-rich layer. When the He flash quenches and the luminosity of the He-burning shell becomes lower than 100 times the surface luminosity, we deactivated the extra energy source. Our results are summarized in Table 5 (lines 1–4): the larger the energy injected into the He-rich layer, the larger the flash-driven convective shell, the larger the mass loss during the RLOF, the more internal the position of the He-burning shell after the RLOF episode and, hence, the lower the accumulation efficiency.

We performed also another test, by putting $\beta = 0$ and preventing the mixing in the flash-driven convective shell. In this way, the He-burning shell is not refuelled, so that the resulting He flash is definitively less strong ($L_{\rm He}^{\rm Max}$ is almost an order of magnitude lower than in the standard case) and the corresponding accumulation efficiency approaches almost unity (line 5 in Table 5). To test the sensitivity of $\eta_{\rm acc}$ on the amount of helium dredged down by convective mixing further, we computed an additional model. In this case, during the phase when the outer border of the flash-driven convective shell coincides with the stellar surface, we artificially altered the chemical composition in the outermost 10^{-6} M$_\odot$ zone of the WD after each time step by restoring the local abundances of all elements as in the accreted matter (see Section 2). In this way, the reservoir of helium-rich matter that could feed the He flash is increased by about 50 per cent. As shown in Table 5 (line 6), the resulting He flash is stronger and, correspondingly, the retention almost halves.

The results of all the toy models listed in Table 5 clearly suggest that the strength of the He flash plays a pivotal role in determining the accumulation efficiency. In fact, it determines the energy content of the He-rich layer in accreting WDs at the onset of the RLOF and, hence, the amount of mass that has to be lost to attain the physical condition suitable for the accreting WD to start its blueward evolution. Moreover, the strength of the He flash determines the maximum inward shift of the He-burning shell during the flash-driven convective episode as well as the duration of the expansion phase up to the RLOF, affecting the exact value of $M_{\rm He}^{\rm R}$. Note that the energy delivered by the He flash is determined mainly by the value of $\dot{M}$ for a fixed initial CO WD, even if our results also demonstrate that the convective mixing acts as a propelling mechanism of the He flash itself, thus affecting the final value of the accumulation efficiency.

Table 6. The same as in Table 4, but for model M092 accreting He-rich matter at $\dot{M} = 5 \times 10^{-7}$ M$_\odot$ yr^{-1} and with different values of the Roche lobe radius, as listed (in solar units).

$R_{\rm Roche}$	$\Delta M_{\rm tr}^1$	$\Delta M_{\rm tr}^2$	$\Delta M_{\rm L}$	$\eta_{\rm acc}$	$M_{\rm He}^{\rm R}$	$\Delta M_{\rm He}^{\rm R}$
0.1	1.426	0.086	0.60	0.594	0.918 63	1.335
1.0	1.444	0.112	0.16	0.895	0.918 86	1.566
10.0	1.450	0.114	0.03	0.983	0.918 93	1.630

For the sake of comparison, in Fig. 6 we also show the values of $\eta_{\rm acc}$ obtained by KH04 in the framework of the optically thick wind scenario for 0.9 (dotted line) and 1.0 M$_\odot$ (dashed line) CO WDs. The differences in the estimated retention efficiency reflect the different assumptions concerning the mass loss episode. To make this issue clearer, recall that the huge energy released during the He flash is stored in the He shell as thermal energy, since the nuclear timescale is shorter than the radiative diffusion timescale due to partial degeneracy of the matter. Hence, the flash-driven convective episode redistributes the thermal energy excess, so that the thermal content of the layer above the He-burning shell increases while its physical dimensions (both in radius and mass) remain practically unaltered. In this way the thermal energy of the He-rich layer becomes too large for its very compact configuration and, hence, it has to be dissipated. Such a situation is similar to what occurs to an ideal gas evolving at constant volume (and, hence, constant density): if the temperature is increased then the pressure has to increase. In an He-flashing structure, the overpressure determined by the increase of the thermal content triggers the expansion of the whole He-rich layer, making work against gravity. In this way the volume increases, the density decreases as well as the specific heat; thus, the thermal content of the He-rich zone decreases. The Roche geometry defines a finite volume in the space so that matter residing inside the corresponding lobe represents the expanding WD while the mass passed through it is lost from the binary system. Hence, due to the continuous expansion, the portion of the star remaining inside the lobe has a lower density and, hence, its specific heat decreases.

In the RLOF model, expansion determines the mass loss, while in the KH04 model wind mass loss is an additional mechanism favouring the reduction of the thermal content of the expanding He-rich layer. As a consequence, for low values of the accretion rate, i.e. for very powerful non-dynamical He flashes, in the RLOF case a larger amount of mass has to be lost and, consequently, the accumulation efficiency is lower than for the KH04 models. For high values of $\dot{M}$, i.e. for less energetic non-dynamical He flashes, in the KH04 computation mass loss starts very soon, when the accretor is still very compact (the surface radius is smaller than 0.1 R$_\odot$), so that in this case the expansion does not play a significant role in reducing the thermal energy excess. On the other hand, in the Roche lobe scenario, the WD continues to expand to larger radii, so that the thermal energy excess in the He envelope is already largely reduced when the mass loss episode induced by the presence of the Roche lobe occurs. As a consequence, in the latter case $\eta_{\rm acc}$ is larger than in the KH04 models. Such a conclusion is confirmed by the values of $\eta_{\rm acc}$ we obtain for an additional set of models, where we compute accretion of He-rich matter at $\dot{M} = 5 \times 10^{-7}$ M$_\odot$ yr^{-1} onto the M092 *heated model* but varying the size of the Roche lobe. As shown in Table 6, the lower $R_{\rm Roche}$, the larger the amount of matter lost from the accretor to remove the thermal energy excess determined by the He flash. It is worth noticing that, if it is

assumed that the strong wind by KH04 is at work, the retention efficiency for all these models should be $\eta_{\rm acc} = 0.858$. Table 6 also reveals that $\Delta M^2_{\rm tr}$ decreases as the Roche lobe radius is reduced. This because, after the RLOF episode, during the blueward excursion along the high luminosity branch of the loop in the HR diagram, the evolutionary timescale becomes longer and a sizable amount of matter can be accreted (see also Table 4). As a consequence, the lower the Roche lobe radius the shorter the time spent in steady burning condition, the smaller the value of $\Delta M^2_{\rm tr}$. Moreover, we found that also $\Delta M^1_{\rm tr}$ depends mildly on the exact value of $R_{\rm lobe}$, as the redward evolution after the end of the flash-driven convective episode is slower with respect to the time span of the He flash itself (see the discussion at the beginning of this section). Our results suggest that in relatively wide systems the accumulation efficiency weakly depends on the radius of the critical lobe, but it may be reduced by up to a factor 2 in extremely tight systems.

To investigate the asymptotic behaviour of CO WDs experiencing strong flashes, we computed a sequence of flashes for each WD mass and $\dot{M}$ combination. For low values of $\dot{M}$ the computation of each flash episode is very time-consuming, due to the large number of models in the sequence because of very small time steps and certain problems in determining the physical structure of the accretor (the models are close to becoming dynamical). For this reason, in some cases we computed just two flash episodes. For each sequence we determine the retention efficiency according to equation (5) and in Fig. 7 we plot the results. A table listing the accumulation efficiency plotted in Fig. 7 is available online. In the M060 and M070 cases, we plot also the values of $\eta_{\rm acc}$ for models accreting at $\dot{M} = 10^{-7}$ M$_\odot$ yr^{-1} and $\dot{M} = 2 \times 10^{-7}$ M$_\odot$ yr^{-1}, respectively, which start their evolution in the mild flash regime and, then, experience strong He flashes (for more details, see Section 3.3).

The thermal content of accreting models, as determined by the accretion history before entering the strong flashes regime, has an important role in determining the actual values of $\eta_{\rm acc}$, as, for example, in AM CVn type systems in which $\dot{M}$ over $\sim 10^6$ yr after the beginning of mass transfer declines from $\sim 10^{-5}$–10^{-6} M$_\odot$ yr^{-1} to $\sim 10^{-8}$ M$_\odot$ yr^{-1} (see Fig. 13). In fact, during the previous evolution, occurring in the mild flashes regime, an extended hot layer is piled up on the initial CO WD. This represents a boundary condition completely different from the small helium layer present as a consequence of the pre-heating procedure. Hence, for fixed $\dot{M}$, in the models that did not have stages of steady burning or mild flashes accretion, the He flash will be stronger, leading to a larger mass loss and, hence, to a lower $\eta_{\rm acc}$. For example, for $\dot{M} = 10^{-7}$ M$_\odot$ yr^{-1}, model M060 has $\eta_{\rm acc} = 1$ when its total mass at the bluest point is equal to 0.7251 M$_\odot$, while, for the same accretion rate, model M070 has $\eta_{\rm acc} = 0.429$ when $M_{\rm tot} = 0.7265$ M$_\odot$. The same is also true at $\dot{M} = 2 \times 10^{-7}$ M$_\odot$ yr^{-1} for the model M070, having $\eta_{\rm acc} = 0.905$ at $M_{\rm tot} = 0.8118$ M$_\odot$, and M081, having $\eta_{\rm acc} = 0.783$ at $M_{\rm tot} = 0.8107$ M$_\odot$. However, pulse by pulse, the thermal content of the He-rich zone is modified, as thermal energy is diffused inward on a timescale depending mainly on the CO core mass. Therefore, the mean temperature level at the base of the accreted He-rich layer becomes a function only of the actual mass of the CO core and of the mass of the helium layer (which is determined by $\dot{M}$ for each value of $M_{\rm CO}$). Therefore, the differences in the accreting models with different accretion histories are smeared off, so that their accumulation efficiency attains an asymptotic value. This is evident when comparing M060 and M070 models accreting at $\dot{M} = 10^{-7}$ M$_\odot$ yr^{-1}, for which we obtain $\eta_{\rm acc} = 0.389$ at $M_{\rm tot} = 0.7649$ and $\eta_{\rm acc} = 0.337$ at $M_{\rm WD} = 0.7645$, respectively. For all these models, the general trend is that, for fixed $\dot{M}$, $\eta_{\rm acc}$ decreases, increasing the total mass of the accreting WDs.

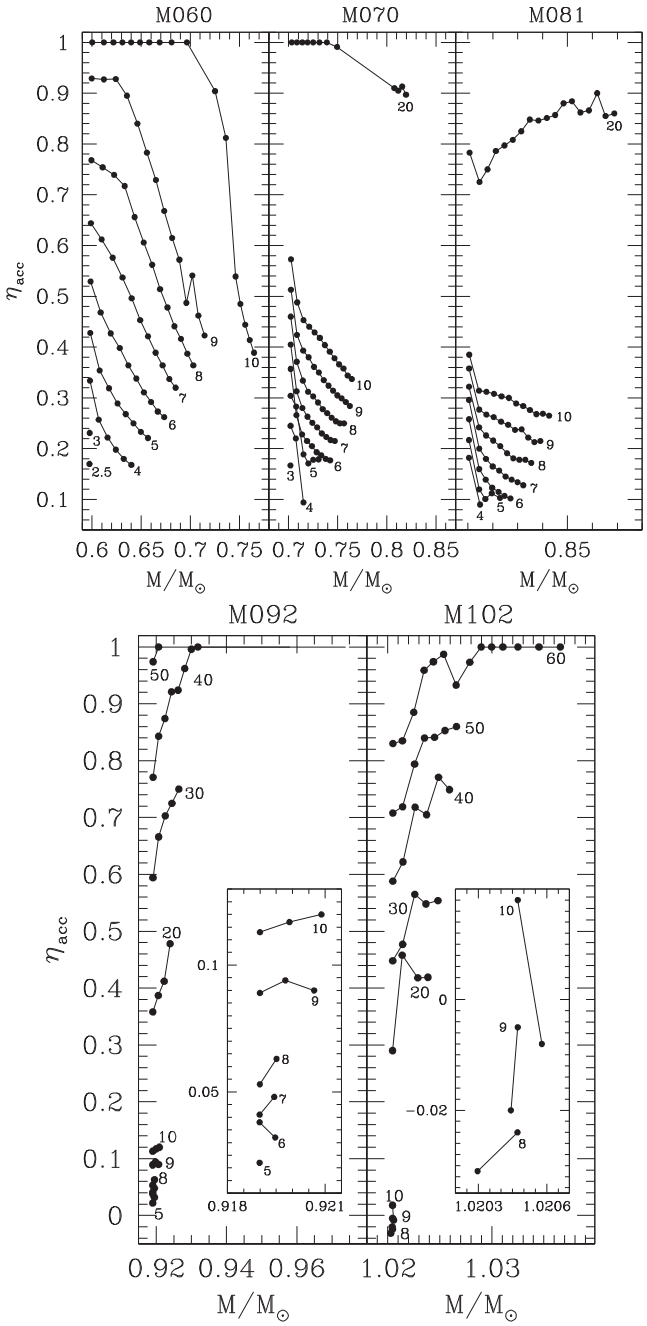

Figure 7. Accumulation efficiency $\eta_{\rm acc}$ as a function of the WD total mass at the bluest point along the loop in the HR diagram, for all the models listed in Table 1. Different curves refer to different accretion rates, as labelled (in 10^{-8} M$_\odot$ yr^{-1}).

These considerations are still valid for more massive initial CO WDs, as can be derived by inspection of Fig. 7. Indeed, for high values of the accretion rate, the accumulation efficiency increases in the M092 and M102 models, since the energy delivered by both the deposition of matter and the He flash is employed to heat the most external layers of the He-deprived core, thus modifying the degeneracy level of the physical base of the He shell. Therefore, pulse by pulse, He flashes become less strong so that the fraction of mass effectively retained during the episode increases. On the other

Table 7. Selected properties of models with the same accretion rate and different initial masses. From left to right we list the initial model, the total WD mass at the bluest point in the HR diagram, the corresponding effective temperature and luminosity, the mass coordinate of the He-burning shell, and the corresponding values of density and temperature. In the last column we report the accumulation efficiency. See text for more details.

Model	$M_{\rm BP}$	$\log(T_{\rm eff})$	$\log(L/L_\odot)$	$M_{\rm He}$	$\log(\rho_{\rm He})$	$\log(T_{\rm He})$	$\eta_{\rm acc}$
			$\dot{M}=10^{-7}{\rm M}_\odot$				
M060	0.736 278	5.477 12	3.856 58	0.731 13	3.6606	8.3296	0.811 64
M070	0.737 064	5.486 64	3.857 90	0.734 11	3.4683	8.2744	0.403 75
			$\dot{M}=3\times10^{-7}{\rm M}_\odot$				
M060	0.920 639	5.652 80	4.215 10	0.919 70	3.3369	8.3352	0.969 85
M070	0.919 911	5.662 84	4.239 22	0.918 64	3.5007	8.3761	0.954 35
M081	0.919 113	5.654 28	4.218 38	0.918 16	3.3541	8.3391	0.949 49
M092	0.919 064	5.684 52	4.243 09	0.918 32	3.3638	8.3507	0.593 58

hand, for low $\dot{M}$, the compressional heating timescale becomes longer than the inward thermal diffusion timescale. Therefore, He flashes are ignited in more degenerate matter and the corresponding $\eta_{\rm acc}$ decreases as $M_{\rm tot}$ increases.

3.3 Mild flashes regime

For slightly larger values of the accretion rate, CO WDs accreting He-rich matter experience mild flashes. In this case, the evolution is similar to models experiencing strong flashes: a He-rich layer is piled up via accretion, determining the compressional heating of the He shell up to the moment when the physical conditions suitable for He ignition are attained. However, as $\dot{M}$ is larger than in the previously discussed case, energy losses cannot counterbalance compressional heating, so that the He shell does not become degenerate at all. As a consequence, the resulting He flash is very mild and it delivers just the amount of energy to determine the transition of the model from the low to the high state. As a result, the radii of CO WDs experiencing this accretion regime typically remain smaller than $\sim$0.5 $R_\odot$, so, excluding the most compact AM CVn stars, no interaction with the companion could occur and all the matter transferred during each cycle is effectively deposited onto the accretors. For AM CVn stars with separations $\sim$0.1 $R_\odot$, formation of a short-living common envelope may be envisioned and then $\eta_{\rm acc}$ should decrease.

It is well known, and we find it as a result of our computations too, that for a given value of the accretion rate, He flashes become stronger, as the total mass of the CO WD increases. As a consequence the models may evolve from the mild flashes regime to the regime of strong flashes. However, the possibility of such a transition depends not only on the actual mass of the accreting WD, but also on the previous accretion history, which, in turn, fixes the thermal content of the CO core. Such an occurrence appears evident when comparing the long-term evolution of models with the same $\dot{M}$ and different initial mass (see Table 7). For example, model M070 accreting at 10^{-7} $M_\odot$ yr^{-1} experiences strong He flashes from the very beginning ($M_{\rm WD}=0.70185$ $M_\odot$), while model M060 accreting at the same $\dot{M}$ enters the strong flashes regime when its total mass has increased to $M_{\rm WD}=0.72514$ $M_\odot$. In the latter model, the deposition of matter has deeply modified the temperature profile in the CO core underlying the He-rich layer with respect to the M070 model, as is clearly seen in the upper panel of Fig. 8, where we plot the temperature profile as a function of density for the two models when their total mass is $\sim$0.737 $M_\odot$. The

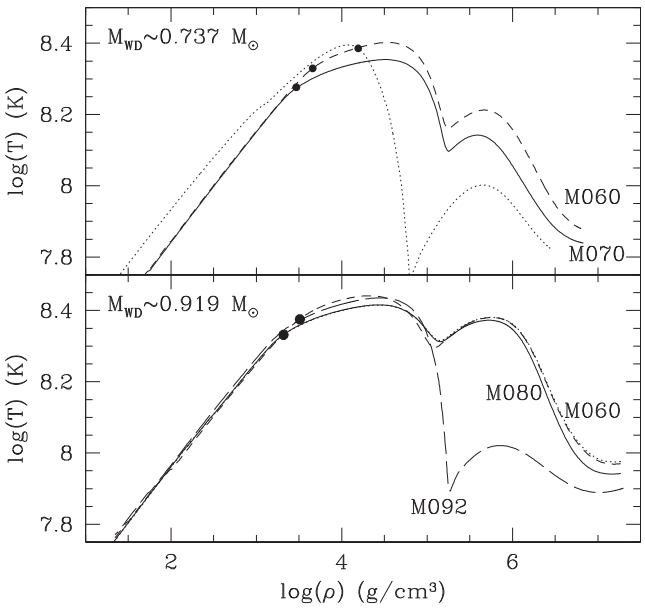

Figure 8. Profiles in the ρ–T for models with the same total mass at the bluest point, but with different initial mass and equal accretion rate ($\dot{M}=10^{-7}$ $M_\odot$ yr^{-1} and $\dot{M}=3\times10^{-7}$ $M_\odot$ yr^{-1} in the upper and lower panels, respectively). Filled dots mark the position of the He-burning shell. In the upper panel, the dotted lines represent the M060 *heated model*.

same considerations are still valid when considering the evolution of a model accreting He-rich matter at $\dot{M}=3\times10^{-7}$ $M_\odot$ yr^{-1}, as is shown in the lower panel of the same figure. Note that in this case, the temperature profiles in the inner zones of the CO cores of models M060 (dotted line) and M070 (dashed line) became practically coincident. It is worth noting that the difference in the temperature profiles of the models with the same total CO core mass and accretion rate, but with different accretion histories, leads to different accumulation efficiencies, as is evident from the last column of Table 7. Some differences between models M060 and M070 are due to the fact that the nuclear energy delivered during the last $\approx$1 Myr of evolution corresponding to the mild flashes regime has been transferred inward very efficiently, so that the entire M060 model became hotter and less dense than the M070 one. As well, the structures do not have exactly the same CO-core mass.

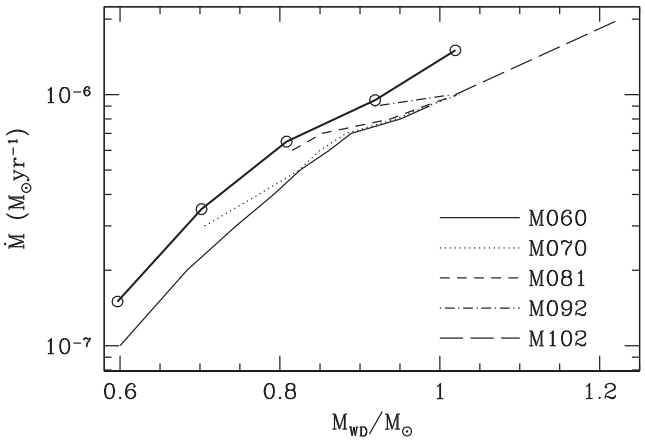

Figure 9. Evolution of the accretion rate at which the transition from steady accretion to the mild flashes regime occurs as a function of the WD total mass. Different lines refer to different initial models. The heavy solid line and open dots are the lower limit of the steady accretion zone shown in Fig. 2.

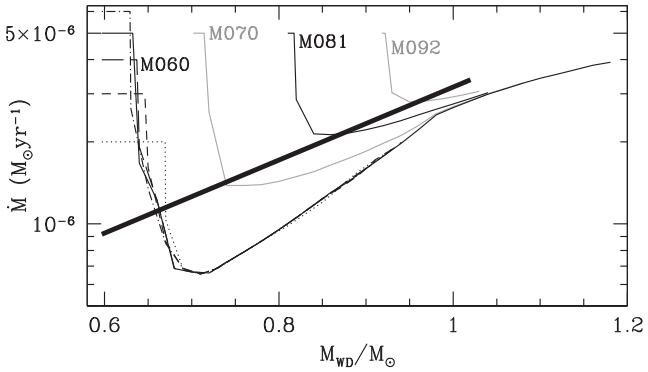

Figure 10. Evolution of $\dot{M}_{RG}$ as a function of WD total mass. Solid lines are for models with different initial mass and the same accretion rate $\dot{M} = 5 \times 10^{-6}$ $M_\odot$ yr^{-1}. Dotted, dashed, long-dashed and dot-dashed lines are for the M060 model accreting He-rich matter at 2, 3, 4 and 6 $\times$ 10^{-6} $M_\odot$ yr^{-1}, respectively. The heavy solid line is the upper limit of the steady accretion zone, as in Fig. 2.

3.4 Steady accretion regime

In the steady accretion regime, by definition, the rate at which He is converted via nuclear burning into a CO-rich mixture is very close to the rate at which He-rich matter is transferred from the donor. As a consequence, models experiencing this regime evolve in the HR diagram along the high-luminosity branch of the typical loop. The long-term evolution of these models is determined by the interplay of two different factors:

(i) With an increase of the mass of the CO core, the luminosity level of the models becomes larger. To counterbalance larger radiative energy losses, the shell has to burn helium at a higher rate. This determines a progressive reduction of the mass of the He-rich mantle.

(ii) The external layers of the CO core are hot and expanded, since they have been piled up via nuclear burning. Contraction of this zone delivers thermal energy, which is an additional source to balance the radiative losses from the surface. Hence, He-rich matter has to be burnt at a lower rate. In any case, for a model with a constant or a decreasing accretion rate, the mass of the He-rich envelope progressively reduces and when it becomes smaller than a critical value, the accretor enters the mild flashes regime.

In Fig. 9 we show accretion rate at which the transition from the steady to the mild flashes regime occurs as a function of the WD total mass. For comparison we also plot the transition line as derived for Fig. 2 (open circles with a thick solid line). This figure reveals that the thermal content of the most external zones of the CO core just below the He-burning shell affects the value of the WD total mass at which the transition occurs. Such a conclusion is reinforced when considering that different initial models converge to the same value when about 0.05–0.1 $M_\odot$ of He-rich matter has been accreted.

3.5 RG regime

If the accretion rate is definitively larger than the rate at which helium is nuclearly processed into a CO-rich mixture, a massive He-rich mantle is piled up. As a consequence, an accreting WD resembles a post-AGB star: the more massive the helium envelope, the lower the effective temperature and, hence, the more expanded the structure. Models in the RG accretion regime evolve redward in the HR diagram, developing very soon a surface convective layer, which penetrates inward as the structure expands. When considering that accreting WDs are components of interacting binary systems, it turns out that, depending on the geometry of the systems, they could overfill their Roche lobe, so that a part (if not all) of the matter transferred from the donor has to be ejected from the binary system.

To define the lower limit in the M_{WD}–$\dot{M}$ plane for the RG regime, we adopt the same procedure as for models in the strong flashes regime. In particular, for each model listed in Table 1, we determine the values of $\dot{M}$ for which the accreting WD expands, thus attaining an effective temperature of 11 300 K. Hence, we assume that the Roche lobe radius of the accretor is equal to 10 $R_\odot$ and we force that $R_{WD} \leq R_{Roche}$ by subtracting mass from the WD. We compute the minimum rate for the RG regime as:

$$\dot{M}_{RG} = \dot{M}_{acc} - \frac{\Delta M_{lost}}{\Delta t}, \quad (6)$$

where $\dot{M}_{acc}$ is the rate at which matter is transferred from the donor, ΔM_{lost} is the amount of mass lost via RLOF and Δt the time step. Our results suggest that for a given initial model, the larger the accretion rate, the more rapid the expansion, so that the transition to the RG regime occurs at smaller WD total mass (see Fig. 10). However, after a short transition phase, all the models with the same initial mass converge to the same limiting value, clearly indicating that $\dot{M}_{RG}$ depends on the thermal content of the CO core as determined both by the compression and the thermal energy flowing inward from the He-burning shell. When comparing models with different initial masses, the same conclusion is still valid.

If an accreting WD is in the RG regime, it is quite reasonable to assume that the mass excess with respect to the maximum value defined by equation (6) is lost by the system. However, the further evolution of this kind of binary systems strongly depends on the amount of angular momentum carried away by the lost matter as it determines the evolution of the separation and, hence, the rate at which the donor continues to transfer mass. As a matter of fact, if the mass transfer occurs at a rate typical of the RG regime, both the components of the binary system should become immersed in a common envelope.

Table 8. Physical properties of some selected models experiencing C ignition. For more details, see the text.

$\dot{M}$ (10^{-6} $M_\odot$ yr^{-1})	$M_{\rm fin}$ ($M_\odot$)	$M_{\rm ig}$ ($M_\odot$)	$\log(\rho_{\rm ig})$ (g cm^{-3})	$\log(T_{\rm ig})$ (K)	$M_{\rm fin}$ ($M_\odot$)	$M_{\rm ig}$ ($M_\odot$)	$\log(\rho_{\rm ig})$ (g cm^{-3})	$\log(T_{\rm ig})$ (K)
	He accreting				CO accreting			
			M102					
2	1.3746	0.0000	9.3230	8.4321	1.3733	0.0000	9.3230	8.4321
3	1.3347	1.3204	6.3845	8.7761	1.3559	1.3445	6.4328	8.7743
			M092					
2	1.3747	0.0000	9.3230	8.4321	1.3740	0.0000	9.3195	8.4358

4 EVOLUTION UP TO C IGNITION

In principle, if the He donor is massive enough, accreting WDs could attain the physical conditions suitable for C ignition. In this regard, it is important to remark that in He-accreting WDs, a part of the nuclear energy released via nuclear burning is transferred inward, though it does not significantly heat the underlying CO core. In fact, the thermal evolution of the CO core is driven by the deposition of CO-rich material, the ashes of the He-burning shell. As a consequence, it can be argued that for values of the accretion rate lower than 1–2 $\times$ 10^{-7} $M_\odot$ yr^{-1}, C burning will be never ignited in He-accreting CO WDs. If CO-rich matter is directly accreted onto CO WDs, for such values of $\dot{M}$ the structure can grow in mass up to the Chandrasekhar mass limit, when the strong homologous compression determines the physical conditions suitable for C ignition at the centre (for example, see Piersanti et al. 2003 and references therein). However, according to the results discussed in Section 3.2, for $\dot{M} \leq 2 \times 10^{-7}$ $M_\odot$ yr^{-1}, He-accreting WDs enter the strong flashes regime, independently of their initial mass, and the amount of matter effectively accreted decreases very rapidly to zero as $M_{\rm WD}$ increases. For this reason, in the considered range of accretion rates, the final outcome is a very massive CO WD.

For larger $\dot{M}$, the extant results for WDs accreting CO-rich matter suggest that central C ignition occurs for $\dot{M} \leq 10^{-6}$ $M_\odot$ yr^{-1}, while for larger values C burning is ignited off-centre (see Piersanti et al. 2003 and references therein). To define the maximum $\dot{M}_{\rm He}$ for which a C-deflagration supernova could occur, we computed the long-term evolution of He-accreting WDs with accretion rates 1–3$\times$ 10^{-6} $M_\odot$ yr^{-1}. The results are summarized in Table 8, where we report the mass coordinate where C burning is ignited, the values of density and temperature at that point and the total mass at the ignition time.[8] In Fig. 11, we plot the profile of the last computed structure in the ρ–T plane for the model M102 accreting at $\dot{M} = 2 \times 10^{-6}$ $M_\odot$ yr^{-1} and $\dot{M} = 3 \times 10^{-6}$ $M_\odot$ yr^{-1} (upper and lower panels, respectively). Solid lines are for He-accreting WDs, while dashed lines are for CO-accreting WDs. As can be noticed, models igniting carbon at the centre have the same physical properties, independently of the chemical composition of the accreted matter. In this case, the evolution up to the ignition is driven by the contraction of the whole accreting WD as it approaches $M_{\rm Ch}$. At variance, the temperature and density profiles in models igniting carbon off-centre depend on the presence of the He-burning shell. In fact, since C burning occurs very close to the surface, thermal energy flowing from the He-burning shell keeps the underlying CO layer hotter.

[8] We define the ignition point as the mass coordinate where the nuclear energy production rate via C burning is equal to the neutrino energy loss rate. The epoch at which such a condition is fulfilled defines the ignition time and, hence, the value of the WD total mass reported in Table 8.

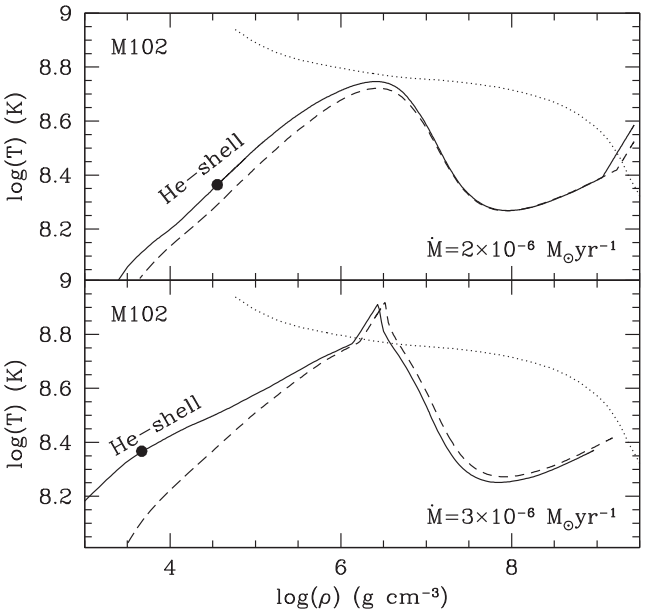

Figure 11. Profiles in the ρ–T plane for some selected models attaining the physical conditions suitable for C ignition. Solid and dashed lines are for He-accreting and CO-accreting WDs, respectively. The location of the He-burning shell in He-accreting models is marked by a filled dot. The dotted line is the ignition line.

According to the previous considerations, central C burning in highly degenerate physical conditions can occur only if $8 \times 10^{-7} \leq \dot{M}_{\rm He} \leq 2 \times 10^{-6}$ $M_\odot$ yr^{-1}. All the He-rich matter accreted in the steady and mild flashes regimes is retained by the WD and determines the growth in mass of the CO core. The matter accreted in the strong flashes regime is only partially retained (when $\dot{M}$ is very low it is not retained at all). When the WD enters the dynamical flashes regime, it could explode if the necessary amount of He-rich matter appropriate to its current mass is accreted.

5 RETENTION EFFICIENCY OF H-ACCRETING WDS

In single-degenerate systems, where the donor has a H-rich envelope, a He-rich layer can be piled up onto the CO WD if the H-accretion rate is larger than the upper limiting rate for the strong nova-like H flashes (e.g. see Cassisi, Iben & Tornambe 1998, and references therein). If H accretion occurs steadily, the rate of H burning and, hence, of He accumulation are by definition equal to the accretion rate. On the other hand, if the H-accreting

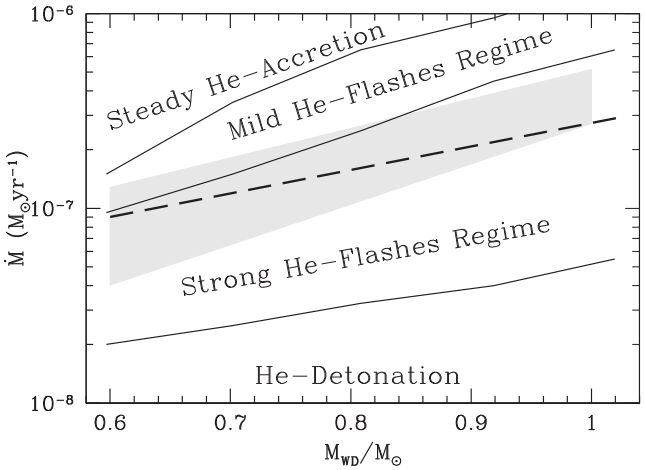

Figure 12. The parameter space suitable for steady accretion of H-rich matter is displayed (grey area) superimposed on the accretion regimes derived in the present work for He-accreting WDs. The heavy dashed line corresponds to equation (7).

WD experiences mild H flashes,[9] the matter accreted before the H flash is nuclearly processed during the high luminosity phase after the H flash so that *averaging* along the loop, the rate of He deposition is almost equal to the rate of H accretion.

Usually the long-term evolution of H-accreting CO WDs is determined by assuming that the behaviour of the He-rich layer is equal to that in a model directly accreting He-rich matter at the same rate. According to the range of $\dot{M}$ values derived by Cassisi et al. (1998) and Piersanti et al. (1999) for the steady H burning and mild H flashes in H-accreting WDs, the helium layer piled up via nuclear burning can undergo either a dynamical or a strong non-dynamical flash. However, on general grounds, the H-burning shell can modify the thermal content of the He-rich zone, so that H-accreting WDs could have an evolution different from those accreting He-rich matter at the same $\dot{M}$. Piersanti et al. (2000) demonstrated that, for low values of $\dot{M}_{\rm H}$, corresponding to the strong He-flashes regime, the mass of the He-rich layer becomes so large that the physical base of the He shell, where the He flash will be ignited, is insulated from the overlying H-burning shell. In this case, the mass of the He-rich zone as well as the temperature and the density at He ignition are practically the same in models accreting H- or He-rich matter at the same rate. On the other hand, Cassisi et al. (1998) showed that for WDs accreting H-rich matter in the steady regime, thermal energy flows from the H-burning shell inward, keeping the whole He-rich zone hotter with respect to models directly accreting He-rich matter at the same rate. As a consequence, in H-accreting models, He burning is ignited when the mass of the He-rich zone is smaller. This might have important consequences in determining the total matter retention efficiency of H-accreting WDs.

[9] Cassisi et al. (1998) assumed that mass loss from an H-accreting model can be triggered by the dynamical acceleration of matter during a nova-like flash or induced by a RLOF for a non-dynamical flash. In the latter case, they described as mild H flashers those WDs that do not expand to giant dimensions after the flash episode, so that all the H-rich matter previously accreted is nuclearly processed piling up a He-rich layer. In more recent work (e.g. Idan, Shaviv & Shaviv 2013; Wolf et al. 2013, and references therein), this classification has been abandoned because the authors take into account the possibility that wind mass loss triggered by the super-Eddington luminosity could occur as a consequence of the H flash.

To illustrate this issue better, we computed some additional models, by accreting H-rich matter onto the M060, M070, M081 and M092 *heated models*. The chemical composition of the accreted matter was set to $X = 0.7$, $Y = 0.28$ and $Z = 0.02$; elements heavier than helium had a scaled solar distribution. Moreover, we assumed that the CO WDs were accreting in the steady H-burning regime at the fixed accretion rate:

$$\dot{M}_H = \left(4.543 \times \frac{M_{\rm WD}}{\rm M_\odot} - 1.817\right) \times 10^{-7} {\rm M_\odot\ yr^{-1}}. \quad (7)$$

In Fig. 12 we show the steady accretion regime for H-accreting models (grey area) as derived by Piersanti et al. (1999), superimposed on possible accretion regimes of He-accreting WDs as derived in Section 3. The long dashed line is the value of $\dot{M}_{\rm H}$ provided by equation (7).

For comparison, we compute also models with the same accretion rate, but with chemical composition of the accreted matter $X = 0$, $Y = 0.98$ and $Z = 0.02$ as in Section 3. In Table 9, we report some relevant quantities of the computed models.

In the M070, M081 and M092 models, the total amount of mass transferred to the WD ($\Delta M_{\rm tran}$) as well as the mass of the He-rich layer at the onset of the He flash ($\Delta M_{\rm He}$) are lower in the H-accreting case. Moreover, due to the flow of thermal energy from the H-burning shell inward, the bottom of the He shell, where the He flash is ignited, is hotter and less dense with respect to the same model directly accreting He-rich matter. As a consequence, in the H-accreting case the He flash is less strong, as suggested by the lower value of $L_{\rm He}^{\rm max}$. Similar considerations are valid also for the M060 case, even if the differences between the H- and He-accreting cases are less marked, because the accreted matter represents a small fraction (∼15 per cent) of the He-rich zone at the onset of the He flash. Due to the He flash, all the models expand to giant dimension, so we assume that the accreting WD fills its Roche lobe when its surface radius becomes larger than $10\,{\rm R_\odot}$. At the onset of the RLOF, we stop the accretion and compute the following evolution up to when the WD definitively contracts. The obtained retention efficiency is listed in the last row of Table 9.

Our results are in good agreement with the findings by Cassisi et al. (1998), while they contradict the recent work by Newsham, Starrfield & Timmes (2013). A direct comparison of the computations in the latter work and our results is possible only for the M070 model accreting at $\sim 1.9 \times 10^{-7}$ M$_\odot$ yr^{-1}, corresponding to the model with $M_{\rm WD} = 0.7$ M$_\odot$, accreting H-rich matter at $\dot{M} = 1.6 \times 10^{-7}$ M$_\odot$ yr^{-1}. In this case, we find that the strong He flash is ignited when a mass of ∼0.008 M$_\odot$ has been accreted onto the WD, while Newsham et al. (2013) halted their computation after the total accreted mass was ∼0.00175 M$_\odot$, i.e. well before the physical conditions for igniting He burning in the He-rich layer could be attained.

Recently, Idan et al. (2013, hereafter ISS13) analysed the very long-term evolution of H-accreting massive WDs. They considered high values of $\dot{M}$, corresponding to steady H burning in a RG-like star and they found that all the computed models experience a very powerful He flash driving the expulsion of the whole accreted He layer. Their models cannot be compared directly with the results of our computations because we consider initial WDs definitely less massive. Moreover, ISS13 included in their computation the effects of the thick wind, which reduces the average value of the accretion rate. For their model with $M_{\rm WD} = 1.00$ M$_\odot$ accreting H-rich matter at $\dot{M} = 10^{-6}$ M$_\odot$ yr^{-1}, the strong He flash occurs when the mass of the He-rich layers attains $\Delta M_{\rm He} = 9.9 \times 10^{-3}$ M$_\odot$, after about 33 000 yr (4153 H flashes with a period of 8 yr). This

Table 9. Selected physical properties of models M060, M070, M081 and M092 accreting H- and He-rich matter at a rate given by equation (7). The listed values of the He-shell position ($M_{\rm He}$), its density ($\rho_{\rm He}$) and temperature ($T_{\rm He}$), the mass of the He-rich ($\Delta M_{\rm He}$) and H-rich ($\Delta M_{\rm H}$) layers refer to the epoch of He-flash ignition. $L_{\rm He}^{max}$ represents the maximum luminosity produced via He burning during the flash episode. In the last row we report the retention efficiency for the computed models.

	M060		M070		M081		M092	
	He acc.	H acc.	He acc.	H acc.	He acc.	H acc.	He acc.	H acc.
$M_{\rm He}$	0.5871	0.5866	0.6983	0.6981	0.8092	0.8090	0.9188	0.9186
ρ_{He} (10^4 g cm^{-3})	4.9218	3.8365	4.6535	3.2002	4.2944	2.8316	5.6805	3.4903
$T_{\rm He}$ (10^8 K)	1.3902	1.7216	1.4458	1.8366	1.5054	1.9540	1.4653	1.9311
$\Delta M_{\rm tran}$ (10^{-2}M$_\odot$)	1.3985	1.4413	0.9268	0.8033	0.5281	0.4460	0.4156	0.3076
$\Delta M_{\rm He}$ (10^{-2}M$_\odot$)	9.2495	9.2780	4.9761	4.5877	1.4159	1.3212	1.1457	1.0369
$L_{\rm He}^{\rm max}$ (10^{42} erg s^{-1})	3.1191	3.0973	7.3273	4.1301	7.8490	5.2372	32.5150	7.4220
$\Delta M_{\rm H}$ (10^{-4} M$_\odot$)	–	2.2862	–	0.9673	–	0.5615	–	0.1640
$\eta_{\rm acc}$	0.659	0.649	0.5209	0.5797	0.6561	0.5928	0.3236	0.4518

corresponds to an average growth rate of the He-rich layer of about $\dot{M}^*_{\rm He} \sim 3 \times 10^{-7}$ M$_\odot$ yr^{-1}. This model can be compared with our M102 model accreting He-rich matter directly at the same accretion rate, even if there are some caveats. The initial model in ISS13 is a bare CO core with a temperature of 6×10^7 K at the centre and $\sim 10^7$ K at the border of the He-deprived core, while in our M102 *heated model*, the CO core is capped by a He-rich mantle and the temperature in the zone below the He-burning shell is larger (see Table 1). Moreover, model M102 has already experienced one very powerful He flash (pre-heating procedure) while ISS13 focus their attention on the very first He flash. Note that in the latter model, the recurrent H flashes experienced by the accreting WD deliver an amount of nuclear energy definitively lower than the pre-heating He flash in our M102 model. This implies that the thermal content of the layer below the He-burning shell in the initial model adopted by ISS13 is definitively lower than in our M102 heated model.

Finally, as discussed at the beginning of this section, the mass of the layer above the He-burning shell at the epoch of the He flash could be lower in WD accreting helium as a by-product of H burning because the thermal energy is diffused inward from the burning shell, thus allowing He to be ignited when a smaller amount of He-rich matter has been piled up. In our model M102 accreting He-rich matter directly at $\dot{M}^*_{\rm He}$, a strong He flash is ignited after the deposition of $\sim 2.12 \times 10^{-3}$ M$_\odot$ of matter; the He flash is ignited at the mass coordinate 1.020 50 M$_\odot$ and the mass coordinate of the He-burning shell moves inward during the flash-driven convective episode down to the mass coordinate 1.020 18 M$_\odot$. Hence, in our model the mass of the He-rich layer above the burning shell is at a maximum of $\sim 2.42 \times 10^{-3}$ M$_\odot$ (see Table 4), a factor $\sim$4 smaller than in the ISS13 computation. In our computation, the maximum temperature attained during the He flash is $T_{\rm He} = 4.87 \times 10^8$ K, while the maximum luminosity delivered via He burning is as high as 1.10×10^9 L$_\odot$ (see Table 5).

Note that the M102 *cool model* accreting He-rich matter at $\dot{M} = 10^{-7}$ M$_\odot$ yr^{-1} has negative retention efficiency (see the discussion in Section 2). At variance, the M102 *heated model* accreting He-rich matter at the same rate has a small but positive accumulation efficiency ($\eta_{\rm acc} \leq 2$ per cent). Such an occurrence shows that the strength of the He flash depends on the physical conditions (mainly the temperature) below the He-burning shell. To verify if the discrepancy between our results and those in ISS13 depends on the thermal content of the adopted initial CO WD, we evolve our M102 *cool model* up to the instant when its temperature at the centre decreases to 4.36×10^7 K and its central density increases to 3.98×10^7 g cm^{-3}. At this epoch the mass coordinate where the He-abundance is larger than 0.01 by mass fraction has a temperature of $\sim 3 \times 10^7$ K. This structure is more similar to the one adopted as a starting model by ISS13, even if the temperature at the physical base of the He-rich layer is a factor of 3 larger. Hence, we directly accrete He-rich matter at $\dot{M}^*_{\rm He}$ and we find that a very strong He flash is ignited at the mass coordinate 1.022 30 M$_\odot$ when the accreted mass is $\sim 7.12 \times 10^{-3}$ M$_\odot$. During the flash-driven convective episode, the He shell moves inward to the mass coordinate 1.020 17 M$_\odot$, so that the mass of the He-rich layer above the He-burning shell is $\sim 7.55 \times 10^{-3}$ M$_\odot$. In this case, the maximum temperature attained during the He flash and the maximum luminosity related to He burning are $T_{\rm He} = 5.31 \times 10^8$ K and 4.73×10^{11} L$_\odot$, respectively. By comparing this last model with the previous one, for a fixed value of $\dot{M}$, the amount of matter to be accreted to trigger a He flash and, hence, the strength of the He flash itself, do depend on the thermal content of the core underlying the point where He burning is ignited. We do not follow the RLOF episode of this additional model, but, according to the discussion in Section 3.2, we can assume that the corresponding value of the accumulation efficiency is similar to the one obtained for the M102 heated model accreting He-rich matter at 8×10^{-8} M$_\odot$ yr^{-1}, i.e. $\eta_{\rm acc} \leq 0$. According to the data in Table 4, this latter model accretes $\sim 7.25 \times 10^{-3}$ M$_\odot$ during the evolution prior to the RLOF episode and the maximum mass of the He-rich layer above the He-burning shell is 7.54×10^{-3} M$_\odot$. Moreover, during the He flash, the maximum luminosity related to He burning is as high as 7.50×10^{11} L$_\odot$. This result confirms that the discrepancy between our findings and those of ISS13 depends only on the thermal content of the initial model. In particular, our M102 heated model has already experienced a strong He flash, which modified the thermal content below the He-burning shell, while the initial CO core adopted by ISS13 is very cold, as they do not adopt any pre-heating procedure.

6 SOME APPLICATIONS

We discuss below several types of binaries with accretion of helium onto CO WDs. Helium WDs and helium stars in close binaries form in the so-called case B of mass exchange, when the stars overflow Roche lobes in the hydrogen-shell burning stage (Kippenhahn & Weigert 1967). During the subsequent evolution, some of them can stably transfer mass to their companion. In this paper, we are interested only in helium WDs and helium stars with the lowest rates of mass transfer, which do not result in formation of the extended envelopes of a WD ($M_{\rm He} \lesssim 1.5$ M$_\odot$).

6.1 CO WDs in semidetached systems with helium WD companions

Helium WD companions to CO WDs have precursors with main-sequence mass $\lesssim$ 2.0–2.5 $M_\odot$. If the timescale of angular momentum loss by a detached pair of He and CO WDs via radiation of gravitational waves is shorter than the Hubble time, the He WD, which has larger radius than its companion, may overfill its Roche lobe, forming an interacting double-degenerate system. Observationally, these systems are identified with AM CVn stars (Paczyński 1967). Nelemans et al. (2001) nicknamed this variety of AM CVn's the WD family. Their precursors may be hidden, e.g. among so-called extremely low mass detached binary WDs with the mass of the visible component $\lesssim$ 0.2 $M_\odot$, a significant fraction of which is expected to lose mass stably after the contact (see Brown et al. 2013, and references therein). Evolutionary considerations and conditions for stable mass exchange, limit initial masses of the donors and accretors in the WD family of AM CVn stars to 0.1–0.3 $M_\odot$ and 0.5–1.0 $M_\odot$, respectively (Nelemans et al. 2001; Marsh, Nelemans & Steeghs 2004; Solheim 2010). As was shown by Tutukov & Yungelson (1996) and Nelemans et al. (2001), the time delay between formation of a detached pair of He and CO WDs and the onset of mass transfer may last from several million years to several gigayears. Therefore, the finite entropy of the WD filling its Roche lobe should be taken into account in evolutionary computations (see Deloye et al. 2007, and references therein).

The non-zero entropy of the donors is reflected in the degree of their degeneracy, which may be characterized by the central degeneracy parameter $\psi = E_{F,c}/kT_c \approx \rho_c/(1.2 \times 10^{-8} T_c^{3/2})$, where ρ_c, T_c and $E_{F,c}$ are the central density, temperature and electron Fermi energy, respectively. The relations between the mass of the donor and the mass loss rate for two systems: ($M_{d,0}/M_\odot$, $M_{a,0}/M_\odot$, ψ) = (0.3, 0.525, 1.1) and (0.3, 1.025, 3.0) are plotted in Fig. 13. The former system is an example of a binary with a hot low-mass donor in which RLOF occurred very soon after formation, while the latter system is an extreme example of a system with a cold donor and massive accretor. Typical evolutionary tracks for AM CVn stars should be located between these two curves. The tracks, computed by a full-scale evolutionary code with realistic equation of state and opacities under the assumption of completely conservative mass exchange, were kindly provided by C. Deloye (see Deloye et al. 2007). Actually, if completely non-conservative evolution is assumed or the mass of the donor is varied to the typical value of an accretor mass 0.2 $M_\odot$, the tracks in the $M_{\rm WD}$–$\dot{M}$ plane practically do not differ. Heavy dots on the lower line in Fig. 13 are the lower limits of $\dot{M}$ for steady burning, and the mild flashes and strong flashes regimes, respectively, as derived in the present study. In the strong flashes regime, the WD experiences about 10 flashes. A WD accumulates $\lesssim$ 0.1 $M_\odot$ before entering the dynamical flashes regime and, since, for a $\simeq$ 0.7 $M_\odot$ WD it is necessary to accrete at least about 0.2 $M_\odot$ for a dynamical flash (see Fig. 3), the latter never happens. Thus, our results confirm that the strongest last flash really should exist, possibly producing a faint thermonuclear supernova (SN .Ia) (Bildsten et al. 2007). But note, none of the observed explosive events suggested to be an SN .Ia have been confirmed so far (Drout et al. 2013).

At the beginning of mass transfer in a system with a more degenerate donor and more massive accretor, the donor loses mass for $\simeq$ 15 000 yr at a rate exceeding the upper limit for the steady burning of He by the WD. The mass lost by the donor in this regime is $\simeq$ 0.087 $M_\odot$, while the accretor may burn only 0.045 $M_\odot$. It is reasonable to assume that the resulting small amount of ejected matter cannot lead to the formation of a common envelope. In the steady

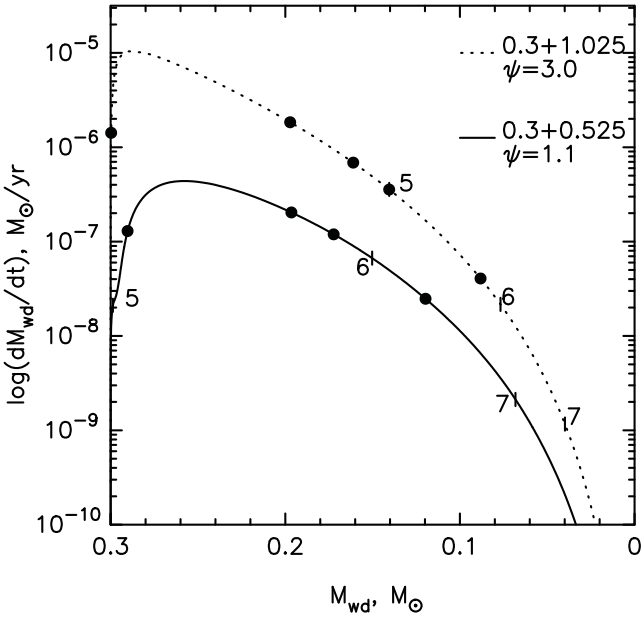

Figure 13. Mass loss rate for finite-entropy He WDs versus their mass in systems with initial masses of donor and accretor $(M_{\rm d,0}, M_{a,0}) = (0.3, 0.525)$ $M_\odot$ (solid line) and (0.3, 1.025) $M_\odot$ (dotted line). ψ is the degeneracy parameter (see text). In the former system $\psi = 1.1$, while in the latter system $\psi = 3.0$. Heavy dots on the upper line mark the $\dot{M}$ limits for RG, steady burning, and the mild and strong flashes regimes (left to right). On the lower line, the same limits for the latter three regimes are marked, since $\dot{M}$ in this case never is high enough for the formation of an extended envelope. Ticks on both lines mark the time elapsed from the beginning of RLOF – 0.1, 1 and 10 Myr, respectively.

accretion, and mild and strong flashes regimes the CO WD may additionally accrete $\lesssim$ 0.1 $M_\odot$. Extrapolation of the data presented in Table 2 suggests that the accretor will experience a dynamical flash. Even if this evolves into a detonation, it is still under debate whether detonation of the He shell results in a double detonation and destruction of the binary (see e.g. Moll & Woosley 2013; Shen & Bildsten 2014). Note, in this case the mass of the accumulated helium may be too high to allow the existing theoretical models to reproduce observations of SNe correctly (Kromer et al. 2010). Such events may be hidden among other transients. As well, they hardly contribute significantly to the total rate of SNe Ia, since AM CVn stars are rare themselves (birth rate $\nu \approx 1 \times 10^{-3}$ yr^{-1}, Nelemans, Yungelson & Portegies Zwart 2004) and typically have low-mass accretors.

It is interesting to note that all the possible explosive events in AM CVn stars happen during the first several million years of their lifetime. This means that currently in the Galaxy there exist only several 10^3 of these binaries that may still be nuclearly active, while the rest may show only accretion-related activity.

However, it is worth noting that, since the delay time between the formation of the CO WD + He WD pair and the beginning of RLOF may be up to several gigayears and the evolution to a dynamical flash regime also proceeds over a gigayear-long timescale, explosions may occur in galaxies of any morphological type.

6.2 CO WDs in semidetached systems with low-mass helium-star companions

For solar chemical composition, the precursors of non-degenerate He-star components in close binaries (with minimum mass

$M_{\rm He} \approx 0.33$ M$_\odot$) have main-sequence mass $\gtrsim$ 2.0–2.5 M$_\odot$. The He-star mass is related to the mass of its main-sequence precursor as $M_{\rm He} \approx 0.08 M_{\rm MS}^{1.56}$ (in solar units). If $M_{\rm He} \lesssim 0.8$ M$_\odot$, the stars do not expand during the core-helium-burning stage, which lasts up to 500–700 Myr. If during this time span, angular momentum loss via radiation of gravitational waves brings the two components into contact, the helium star may fill its Roche lobe and, if the conditions for stable mass loss are fulfilled, mass transfer onto the companion starts. In systems with a CO WD, these stars first evolve to have shorter orbital periods $\simeq$ 10 min. By the epoch of the period minimum, the masses of the He stars decrease to 0.20–0.25 M$_\odot$ and they start to lose matter that was nuclearly processed in their convective cores prior to contact [RLOF quenches nuclear burning very fast (Savonije et al. 1986)].

Semidetached low-mass He star + CO WD binaries also are suggested to be a variety of AM CVn type stars (Savonije et al. 1986; Iben & Tutukov 1991; Tutukov & Yungelson 1996), nicknamed the He-star family (Nelemans et al. 2001). Typical mass transfer rates in these systems before the period minimum are $\lesssim 10^{-7}$ M$_\odot$ yr^{-1} (Yungelson 2008, see also Fig. 14).

In Fig. 14 we show three examples of evolutionary tracks of He stars in semidetached systems with WD companions from Yungelson (2008), in the mass of the donor versus the mass-loss rate plane. The tracks shown in Fig. 14 were computed using a conservative approximation, but this does not affect their behaviour compared to the completely non-conservative case (Yoon & Langer 2004; Yungelson 2008). The initial combination of masses $(M_{\rm He\star}, M_{\rm WD}) =$ (0.35, 0.6) is deemed to be typical for precursors of He-star AM CVn systems, while (0.4, 0.8) M$_\odot$ and (0.65, 0.8) M$_\odot$ may be more rare (see fig. 3 in Nelemans et al. 2001). For each combination of He star and CO WD mass in Fig. 14, we show three characteristic tracks corresponding to the RLOF by a completely unevolved star (line a), a star where He in the core has been consumed by about 40–60 per cent (line b) and a star with a significantly He-depleted core ($Y_c \simeq 0.1$, line c); for lower Y_c, overall contraction begins and the stars cannot fill their critical lobes. Shaded regions in the plots show the domain of strong He flashes (after Fig. 2 above). The lower border of this region is drawn under the assumption that He accretion occurs conservatively, i.e. the mass of the WD is the sum of its initial mass and the mass lost by the He star. For stars experiencing strong flashes, the border between the dynamical and strong flashes regimes is between the shaded regions and dotted lines, representing the transition for completely non-conservative evolution.

In the (0.35 + 0.6) M$_\odot$ set of systems, the accreted He never experiences a dynamical flash since such systems predominantly evolve into the strong flashes regime of He burning immediately after the RLOF. Moreover, the donor is not massive enough to provide enough mass for a dynamical flash after entering this accretion regime (see Table B2 in the Additional material in the online version).

In the (0.4 + 0.8) M$_\odot$ set of systems, the accreting WDs stay in the range of mass-exchange rates corresponding to the dynamical flashes regime for a part of the pre-period-minimum time, but hardly accumulate enough He to give rise to a dynamical event (Fig. 3). In the strong flashes regime, they experience $\simeq$10 outbursts and, even if the corresponding retention efficiency is small, the WD mass should increase. For this case we may safely assume that by re-entering the dynamical flashes regime the total mass of WDs is close to 1.0 M$_\odot$. Then, WDs of this set should experience a dynamical flash shortly after the period minimum, when several 0.01 M$_\odot$ have been accreted. According to Fink et al. (2010), the

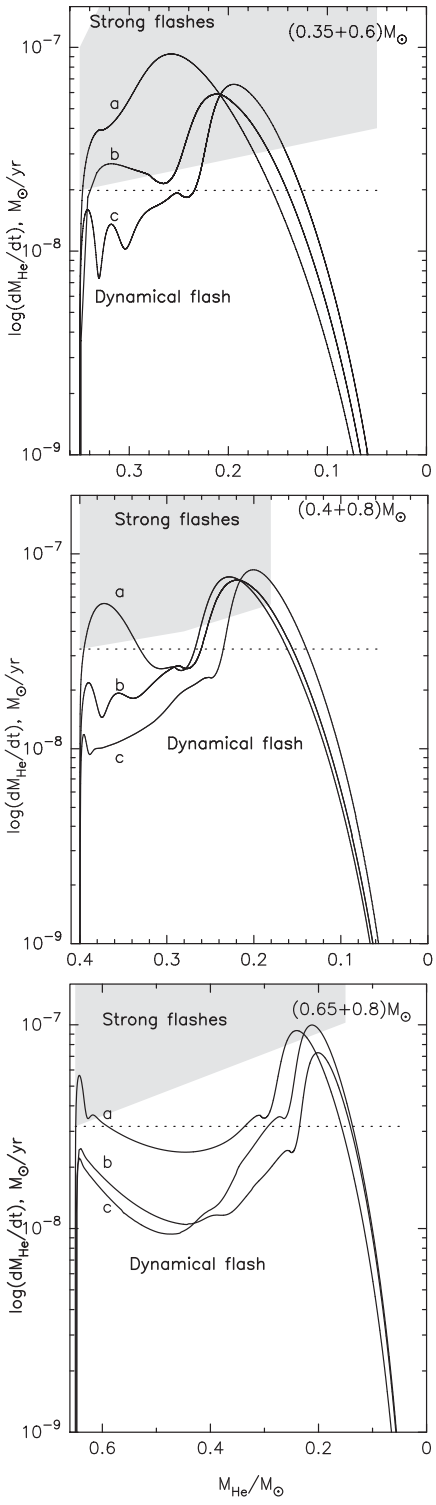

Figure 14. Mass loss rate by non-degenerate He donors in $(M_{\rm He\star}, M_{\rm WD})$ binaries versus mass of the He star. Upper panel shows a (0.35, 0.6) M$_\odot$ pair; lines a, b and c show evolution of the systems with initial period P_0 and He-abundance in the core of (20 min, 0.98), (100 min, 0.64) and (144 min, 0.118), respectively. Middle panel is the same for a (0.4, 0.8) pair, with (20 min, 0.98), (100 min, 0.51) and (140 min, 0.09). Lower panel is the same for a (0.65, 0.8) pair, with (35 min, 0.98), (80 min, 0.4) and (85 min, 0.29). In the shaded regions of the plots, He burns in the strong flashes regime (their lower limits correspond to a completely conservative evolution, while dotted lines mark the same limit for completely non-conservative evolution).

detonation of the He shell in this case may initiate the detonation of carbon close to the centre of the CO WD.

Finally, in the most extreme case of the $(0.65 + 0.8)\,M_\odot$ systems, no strong flashes happen, but dynamical flashes of He onto WD may occur and double detonations may be expected.

Like semidetached WD + WD systems, low-mass He stars evolve to the period minimum in $\sim 10^6$–10^7 yr only. This may mean that most of the AM CVn stars of the He-star family existing in the Galaxy have already experienced their last flash (or SN .Ia for a detonation) and continue to evolve without any expected thermonuclear events. It is possible that some would-be AM CVn's ceased to exist due to double detonations shortly after their birth. The estimation of the rate of the latter events should be addressed by means of population synthesis calculations, taking into account relations between critical masses for explosive events, retention efficiency and $\dot{M}$, which has not be done so far. The same, in fact, is true for the total population of AM CVn's, since in the existing studies their formation rate was restricted by rather *ad hoc* assumptions, while the effects of unstable He burning were not taken into account. The relevance of such a new study is also emphasized by the fact that the existing theoretical models predict significantly larger Galactic population of AM CVn stars than observed and it has been suggested that the theoretical models overestimate their number (see e.g. Carter et al. 2014, and references therein).

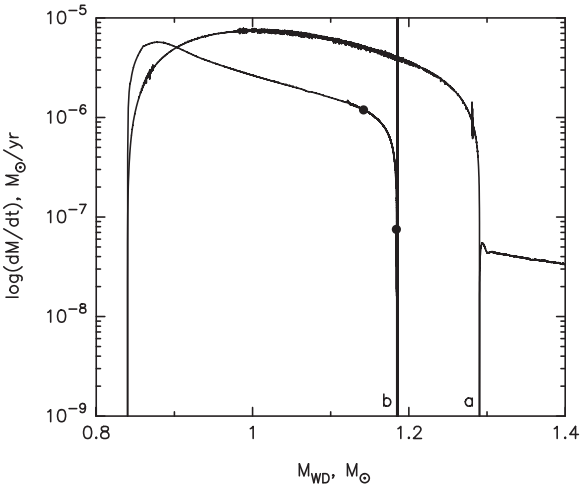

Figure 15. Mass loss rate versus mass of non-degenerate He-donors in semidetached systems with initial masses $M_{He\star,\,0} = 1.23$ $M_\odot$ and $M_{WD,\,0} = 0.84$ $M_\odot$ and initial periods 0.035 d (line a) and 0.2 d (line b). Heavy dots on line b mark the limits of the strong flashes regime. A spike of $\dot{M}$ in line b shows the initial stage of mass transfer in the system formed by the WD remnant of the He star and the CO WD.

6.3 Helium-star channels to SN Ia

Above, we discussed the evolution of CO WDs accreting He from low-mass stellar companions ($\lesssim 0.8$ $M_\odot$), which do not expand after exhausting He in their cores. More massive He stars may overflow the Roche lobe both in the core-He-burning and in the He-shell-burning phases (Paczyński 1971). In the latter case, the expansion (up to several 100 $R_\odot$), which occurs in the thermal timescale, is limited only by the existence of a companion. It has been shown, e.g. by Iben & Tutukov (1985), Yoon & Langer (2003) and Wang et al. (2009), that upon RLOF both core- and shell-He-burning stars may lose several 0.1 $M_\odot$ at a rate $\sim 10^{-(6\pm1)}$ $M_\odot$ yr^{-1}, which corresponds to the accreting CO WDs burning helium in the steady or flashes regimes, depending on the orbital period and combination of masses of the components. If RG formation is avoided, initially sufficiently massive CO WD components may accumulate to M_{Ch}.

As examples of possible evolution, we show in Fig. 15 the M_{WD}–$\dot{M}$ dependence for a system harbouring initially a 1.23 $M_\odot$ He star and a 0.84 $M_\odot$ WD.

We consider two cases: (i) with initial period of the system $P_{orb,\,0} = 0.035$ d, the donor overflows the Roche lobe practically unevolved ($Y_c \approx 0.979$); and (ii) with $P_{orb,\,0} = 0.2$ d, $Y_c = 0$ and the mass of the He-depleted core 0.692 $M_\odot$.

For the unevolved donor, a short ($\Delta T \approx 0.155$ Myr) episode of mass transfer occurs. The accretion rate corresponds subsequently to RG, steady burning, and the mild and strong flashes regimes. The amount of matter transferred in the RG regime is close to 0.2 $M_\odot$ and the question of whether a common envelope may form, if optically thick winds are not considered, remains open. The mass accreted by the WD is not sufficient to attain M_{Ch}. High mass transfer results in a sharp decrease of the nuclear burning rate, and the donor contracts and detaches from the Roche lobe. Since the system is very tight, angular momentum loss via radiation of gravitational waves continues to shrink the orbit. At a certain moment, the Roche lobe radius becomes smaller than the radius of the star and mass loss resumes. The rate of accretion corresponds now to the regime of dynamical flashes. The accreting WD is massive enough to experience a flash virtually immediately after resumption of mass transfer (the mass-loss curve for the second stage of mass transfer is, in fact, formal).

For the evolved system, the mass-loss stage reduces to a rapid ($\Delta T \approx 0.18$ Myr) loss of most of the He layer overlying the CO core. Mass loss does not result in quenching of shell-He burning, the core continues to grow and the remnant of the donor has a 0.831 $M_\odot$ He-depleted core, while its total mass is 0.886 $M_\odot$. It is important to remark that in the strong flashes regime, the donor loses about 0.015 $M_\odot$, while the critical mass of the He layer for ignition, as suggested by extrapolation of the data in Fig. 7 (see also Table B7), is about an order of magnitude lower. Thus, the WD may experience $\sim$10 strong flashes, which may be associated with a helium nova (see Section 6.4). The mass accumulated by the WD may be enough for a dynamical flash when the accretion rate drops into the appropriate range.

Double detonation has been considered as a possible explosion mechanism of SNe Ia for more than three decades (see Section 1). In particular, Wang et al. (2013) suggested that double detonations onto sub-Chandrasekhar WD in He star + CO WD systems produce subluminous supernovae of the SN Iax subtype (Foley et al. 2013). Observationally, SNe Iax are suggested to constitute about 1/3 of all SNe Ia. Note, these events should not currently occur in early-type galaxies and, really, none have been detected in the elliptical ones. Indeed, the evolutionary scenario suggested by Wang et al. is similar to the one discussed in Section 6.2, but involves also more massive donors (up to 1.25 $M_\odot$); an exemplary evolutionary track for this kind of system is curve b in Fig. 15. However, the estimated contributions of pertinent SN Ia to the total rate of SNe Ia in BPS studies, as usual, depend on assumptions in the BPS codes. In particular, Wang et al. assumed that the only condition for the occurrence of a double detonation is accumulation of 0.1 $M_\odot$ of He at a rate between 1×10^{-9} and 4×10^{-8} $M_\odot$ yr^{-1}on a 0.8–1.2 $M_\odot$ WD, irrespective of how robustly the resulting dynamical He flash at these conditions leads to an SN Ia. The possibility of strong flashes was neglected. Note that, also in this case, reproducing the observed features of an SN Iax, apart from being faint,

is still questionable (Kromer et al. 2010). Moreover, the current Galactic star formation rate of 3.5 $M_\odot$ yr^{-1} assumed in the Wang et al. computations is higher than modern estimates, which are close to 2 $M_\odot$ yr^{-1} (Kennicutt & Evans 2012). Finally, as mentioned before, CO WDs hardly form with a mass exceeding 1.1 $M_\odot$. Wang et al. claim that Galactic rates of double detonations in the considered systems are $\sim 1.5 \times 10^{-3}$ yr^{-1}, while a more realistic estimate based on the data in the quoted study and in the present work, hardly exceeds 10^{-4} yr^{-1}.

The possibility of accumulation of $M_{\rm Ch}$ by a He-accreting WD was studied most recently by Wang et al. (2009) by means of BPS, using He-retention efficiencies from KH04. While Wang et al. claim that the He-donor channel may enable ∼30 per cent of the observed SNe Ia rate, we should note again that this result depends very strongly on the assumption that an optically thick stellar wind from the accreting WD operates in the RG regime, thus preventing the formation of common envelopes, and on the limits set for the different accretion regimes. In the quoted study, the mass of the donors in systems with WDs accumulating $M_{\rm Ch}$ may be as high as 2.5 $M_\odot$, while our test calculations, performed by relaxing the assumption of existence of the optically thick wind, show that the maximum mass of the donors is about 1.25 $M_\odot$. For larger masses, the initial $\dot{M}$ corresponds to the RG accretion regime and the formation of common envelopes is expected. We note also that in the study by Wang et al., a significant fraction of SNe Ia is produced by WDs with initial masses between 1 and 1.2 $M_\odot$ and the problem of the origin of very massive CO WDs is not considered. Moreover, the birth rates of binaries that contribute to this channel, i.e. have proper $M_{\rm He}$, $M_{\rm WD}$ and $P_{\rm orb}$, heavily rely on the assumed parameters in a specific BPS code, especially, on the ejection efficiency of the common envelopes, the estimates of the binding energy of the donors and the treatment of the mass transfer process in BPS. For instance, Branch et al. (1995) find that the He-star channel cannot contribute more than several per cent to the current rate of Chandrasekhar-mass SNe Ia in the Galaxy. These systems could be more important in the early stages of the Galactic evolution when the star formation rate was much higher than the current one, since their delay time is limited by the sum of lifetimes of the least massive He donors and their precursors (≈150 Myr).

In this scenario, the amount of mass that can be transferred by a He star onto the CO companion and retained by the latter is crucially important for the helium-ignited violent merger scenario for SNe Ia (Pakmor et al. 2013), since, as noted in the Introduction, exploding WD accretors should be massive (see discussion in Ruiter et al. 2013). We recall, however, that the evolution of He star + CO WD systems has been very poorly explored; some combinations of a He star and WD evolve differently than assumed in population synthesis studies, as demonstrated by Fig. 15. Full-scale evolutionary calculations of stellar models and their parametrization in population synthesis codes produce both different $\dot{M}$ and amounts of mass lost by the He star ($\Delta M_{\rm He}$). For instance, compare full-fledged evolutionary computations for a 6.95 $M_\odot$ star by Iben & Tutukov (1985) and parametrized calculations for a 6.67 $M_\odot$ star in Ruiter et al. (2013): in the latter $\Delta M_{\rm He}$ is more than twice as large as in the former: 0.46 $M_\odot$ versus 0.21 $M_\odot$, thus, it is much more favourable for the He-ignited violent merger scenario. Another issue is whether the amount of mass in the He skin(s) of merging WDs is sufficient for ignition of initial He detonation. In evolutionary computations, nascent CO WDs entering the cooling sequence retain only traces of He at the surface (<0.001 $M_\odot$, Iben & Tutukov 1985). Pakmor et al. (2013) postulate the presence of 0.01 $M_\odot$ of He atop CO cores of merging WDs.

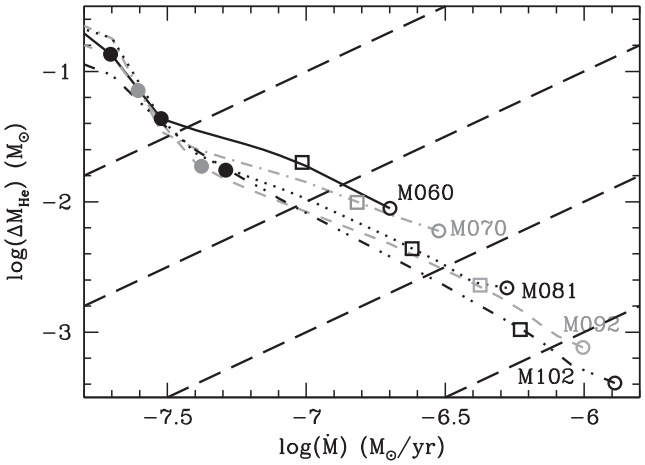

Figure 16. Dependence on the accretion rate of the mass of the He-rich layer above the He-burning shell at the onset of the first He flash for all the models computed in the present work. Different lines are used for different initial WD models, as labelled. Transitions from one accretion regime to another are marked with different symbols: open circles – from steady to mild flashes regime; open squares – from mild to strong flashes regime; filled circles – from strong to dynamical flashes regime. Slanting long dashed lines show recurrence periods from 10^3 to 10^6 yr (bottom to top).

6.4 He novae

In the strong flashes regime, He-accreting WDs probably manifest as He novae – an analogue of novae associated with thermonuclear runaways onto WDs accreting hydrogen (Kato, Saio & Hachisu 1989). In Fig. 16, we show the dependence of He-ignition masses (masses above the coordinate of maximum $\epsilon_{\rm nuc}$) on mass accretion rate. The $\Delta M_{\rm He}$ shown in the figure are lower than the ones computed by Kato et al. (2008) for similar combinations of $\dot{M}$ and masses and so the recurrence time of flashes is shorter.

Helium novae are represented to date by only one still not well-studied object – V445 Pup (Ashok & Banerjee 2003; Woudt & Steeghs 2005; Iijima & Nakanishi 2008; Woudt et al. 2009) and several candidate objects that show similar light curves and over-abundance of He (Rosenbush 2008). V445 Pup apparently, does not belong to the He-star family of AM CVn stars. Woudt et al. (2009) found that the pre-outburst luminosity of the object was $\log(L/L_\odot) = 4.34 \pm 0.36$. Such a luminosity is compatible with the donor being a 1.2–1.3 $M_\odot$ star burning helium in a shell. If the variability of the system with period ≈0.65 d (Goranskij et al. 2010) reflects the orbital motion in the system, it favours such an interpretation. Kato et al. (2008) inferred that the WD component of V445 Pup is very massive ($\gtrsim$ 1.3 $M_\odot$), based on the fitting of the observed nova light curve in the framework of the optically thick wind theory. Based on the test calculations presented in Fig. 15, we may suggest that the initial mass of the WD in V445 Pup could have been close to 0.8 $M_\odot$, while now it is about 1 $M_\odot$.

The apparent extreme rarity of He novae may be due to the low birth rate of systems with an initially massive enough WD and the short duration of the He-shell-burning stage. Regretfully, the real orbital period of the system is unknown, thus hampering the identification of a possible companion to the WD.

7 FINAL REMARKS

We explored systematically the thermal response of non-rotating WDs to direct accretion of helium. The initial WD masses adopted

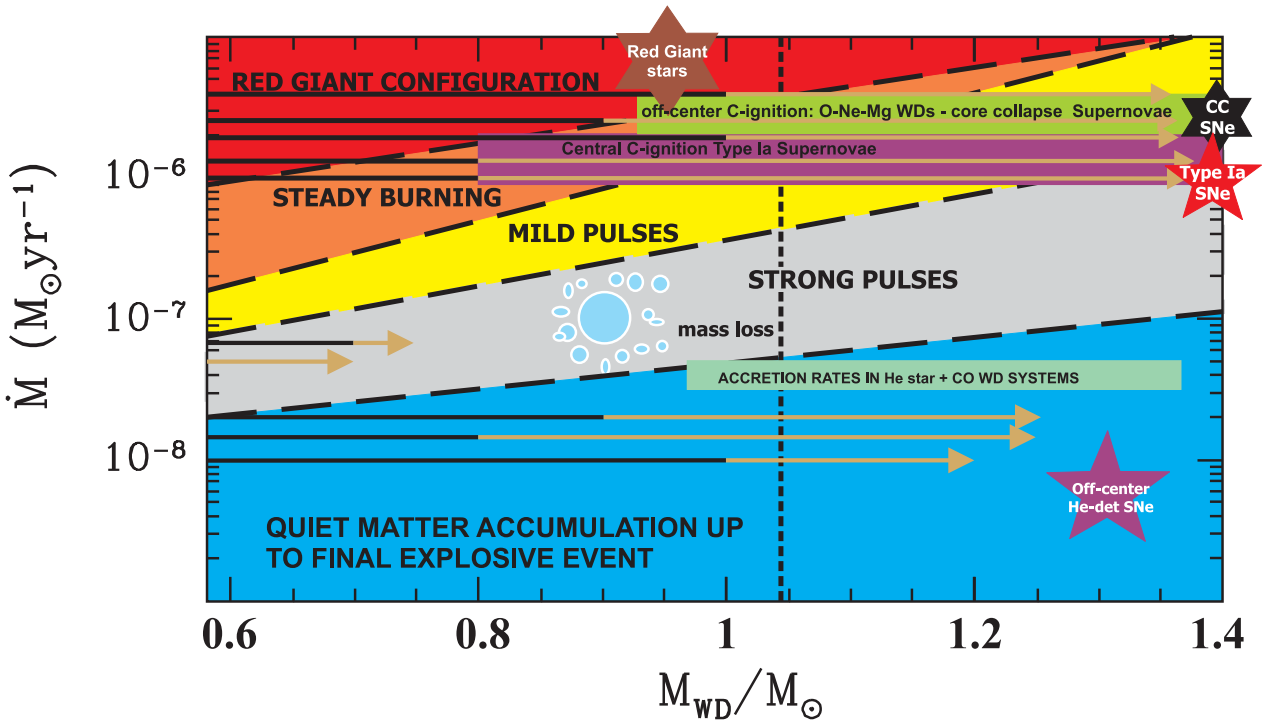

Figure 17. Accretion regimes for He-accreting WDs as a function of the WD total mass ($M_{\rm WD}$) and the accretion rate ($\dot{M}$). The limits of the different accretion regimes on the left of the dotted vertical line have been extrapolated from the results of our computations. The possible final outcomes of the accretion process are also displayed. Black horizontal lines represent the initial WD masses while dark-yellow arrows trace the accretion process.

in our analysis cover the whole range of CO WDs expected to form in close binaries due to mass loss by AGB components – from 0.6 to 1.02 $M_\odot$. As well, the range of studied accretion rates encompasses an evolutionary significant range (1×10^{-9} to 2×10^{-6} $M_\odot$ yr^{-1}). Special attention was paid to the processes involved in energy exchange between the underlying CO core and accreted He layers. Unlike previous studies, in accretion regimes driving the expansion of the WD, due to either thermonuclear flashes at the base of the accreted layer or the WD's inability to consume nuclearly all accreted matter, we considered the possibility of mass and angular momentum loss from the system as determined by the interaction of the WD envelope with the companion.[10] For convenience of discussion, in Fig. 17 we reproduce different evolutionary models involving direct He accretion at constant $\dot{M}$ on a plot showing different burning regimes for He-accreting WDs. Note, the abscissa has been extended up to 1.4 $M_\odot$ to show different pathways to SNe Ia. The limits of the various accretion regimes for WD total masses larger than 1.05 $M_\odot$ (the zone in the plot on the right of the dashed vertical line) have been extrapolated on the base of the results presented in Sections 3 and 4.

In agreement with previous studies, we found that, at *constant* low accretion rates (from $\lesssim 5 \times 10^{-8}$ $M_\odot$ yr^{-1} for 1.02 $M_\odot$ WDs to $\lesssim 2 \times 10^{-8}$ $M_\odot$ yr^{-1} for 0.6 $M_\odot$ WDs), the accretion timescale is much longer than the inward thermal diffusion timescale, so that conditions at the base of the He layer are defined by the interplay between neutrino cooling and energy release by contraction of accreted matter. Helium is deposited quietly at the surface of the CO dwarf and piled up for a long time without an increase of surface temperature and luminosity, while the temperature at the base of the He shell increases. He ignition occurs in highly degenerate matter and it becomes dynamical by its nature. We found that the minimum masses of He accumulated prior to the dynamical flash are 0.02 $M_\odot$ to 0.102 $M_\odot$ for 1.02 $M_\odot$ to 0.8 $M_\odot$ WDs, respectively (Table 2). These masses of accreted He are rather close to the minimum values of $\Delta M_{\rm He}$ that can robustly trigger double detonations in WDs of these masses (Fink et al. 2010). Such events may happen in AM CVn type systems with He-star donors. In Fig. 17, we show three examples of evolutionary tracks for WDs of different initial mass with $\dot{M}$ in the range 1–3 $\times$ 10^{-8} $M_\odot$ yr^{-1} accumulating critical layers for a dynamical event.

The estimates of the contribution of double detonations to the total SNe Ia rate are controversial. On one hand, BPS for precursors of AM CVn stars by Nelemans et al. (2001) with parameters reproducing the population of WD binaries in the Galaxy, shows that a double-detonation SNe Ia should be a very rare outcome, since binaries with massive enough accretors and He star or He WD donors enabling an appropriate accretion rate are hardly formed. On the other hand, Ruiter et al. (2011) found that, for certain combinations of BPS parameters, double detonation of sub-Chandrasekhar WDs may be a dominating mechanism for SNe Ia with delay times shorter than about 5 Gyr; they also found two distinct groups of precursors: short-living ones, harbouring He-star donors, and long-living ones, with He WD donors. Similarly, massive accretors and the high rate of double detonations in He-star AM CVn systems were found by Wang et al. (2013). The reliability of certain sets of results could be demonstrated if, for the same sets of BPS input parameters used to model SNe Ia, it is possible to reproduce the well-observed and numerous enough groups of stars preceding SNe Ia in evolutionary path, like local samples of WD binaries. It is worth noting again that the extant calculations for double-detonating WDs still fail to

[10] To our knowledge, this mode of mass loss was studied by Iben & Tutukov (1996) for a single example of a 1 $M_\odot$ accretor only.

reproduce all SNe Ia observables (Kromer et al. 2010). In Appendix A2 we provide polynomial fits of $\Delta M_{\rm He}$ necessary for a dynamical flash as a function of the accretion rate. Failed double detonations, i.e. single detonations of He that do not trigger explosion of the underlying core, may be hidden among weak SN Ia or other transients with magnitudes between those of novae and supernovae (Kasliwal 2012).

For higher $\dot{M}$, we find the limits of He burning in the strong flashes regime. For semidetached systems composed of low-mass He stars and WD donors with evolution driven by radiation of gravitational waves, an almost constant accretion rate may be a fair approximation in the stage before the minimum of the periods is reached (Yungelson 2008). For systems with He WD donors and CO WD accretors, a decaying $\dot{M}$ is typical. For a decaying mass transfer rate, we show that the amount of matter accumulated prior to the strong flash is a function of accretion history, with $\dot{M}$ being a deciding factor. This zone may be associated with He novae, of which one object is confirmed today (V445 Pup) (Ashok & Banerjee 2003). For stars in this zone, the strong mass loss is typical. If $\dot{M}$ is close to the transition line between the strong and dynamical flashes regimes, the retention efficiency may be negative. This happens because, during the previous evolution, He burning did not attain the surface of the accreting WD, so that a small He-rich zone remained on the top of the CO core. Hence, a negative $\eta_{\rm acc}$ implies that the He flash is ignited in this pre-existing helium layer and, moreover, that almost all the matter above the ignition point is ejected.

The values of retention efficiency we obtained are, for WDs of the same mass, lower than the ones by KH04. We explain this as the consequence of the assumption that mass loss from the system is the result of the interaction of the WD bloated envelope with the companion, while KH04 account for mass loss from the accretor according to the optically thick wind theory. Polynomial fits to the obtained values of retention efficiencies ($\eta_{\rm acc}$) as a function of the accretion rate are provided in Appendix A3.

In SD systems with a H-rich donor, if the accretion proceeds in the regime of steady H burning, accumulation of helium via nuclear burning occurs at a rate typical for the strong He flashes regime. In this case, the comparison between models accreting He directly or as a consequence of H burning at the same $\dot{M}$ shows that in the latter case the mass of the He-rich zone is lower at the onset of the He flash, due to the presence of the H-burning shell, which keeps the underlying He-layer hotter. In any case, the resulting accumulation efficiencies are very similar. It is worth noting that, according to BPS, the H-rich SD scenario cannot account for the observed rate of SNe Ia unless unrealistic unlimited accumulation of hydrogen onto CO WDs is assumed (see the discussion in Claeys et al. 2014).

The next two regimes of He burning are those of mild flashes and steady burning. Mild flashes occur if ignition starts in a non-degenerate matter. The increase of the WD radius is not large and the accumulation efficiency is close to 1. In the steady burning regime, He is converted into a C+O mixture at a rate equal to $\dot{M}$. A caveat is that steady burning is attained only after a strong initial pulse has been experienced by the accreting structure in order to settle the external matter in a thermal equilibrium appropriate for accreting and burning deposited matter. The steady burning and mild flashes regimes open windows in the space of parameters suitable for accreting WDs to evolve up to an explosive final state. For instance, an accreting dwarf may experience steady accretion during the first stage of the evolution and afterward enter the mild flashes regime, thus accumulating mass up to the Chandrasekhar limit. Five detailed evolutionary tracks have been followed in this area, which end with carbon ignition. The models with initial WD mass from 0.8 $M_\odot$ to 1.02 $M_\odot$ with a lower accretion rate succeed in igniting carbon in a deeply degenerate environment and an explosive outcome is attained. For slightly higher values of $\dot{M}$, the maximum temperature is off-centre so that carbon is ignited in an external layer. In this case, it can be argued that C burning propagates inward via heat conduction, transforming the CO core into an O-Ne-Mg one (Saio & Nomoto 1985, 1998). Such a structure, while accretion continues, will experience an accretion-induced collapse into a neutron star. Those windows of outcomes are very narrow in the accretion rate range of parameters when constant $\dot{M}$ is assumed. The most important requirement to get C ignition as a final outcome is that the strong He flashes are avoided. The windows of opportunities can get larger if accretion rates can change during accretion. Results of BPS by Wang et al. (2009) suggest that this channel may be responsible for about 30 per cent of SNe Ia, given that there exists an appropriate observed population of sufficiently massive He stars ($M_{\rm He} \gtrsim 0.8$ $M_\odot$) with massive WD companions ($M_{\rm WD} \gtrsim 1.0$ $M_\odot$) and that the formation of common envelopes at accretion rates exceeding $\dot{M}_{\rm RG}$ may be avoided (see Section 6.3).

Finally, for accretion rates from 10^{-6} $M_\odot$ yr^{-1} for 0.6 $M_\odot$ WD to 3.5×10^{-6} for 1.02 $M_\odot$, the mass deposition onto the WD delivers a huge amount of gravothermal energy. The consequence is that the transferred matter forms an extended envelope acquiring the shape of a RG. The whole structure becomes embedded in the common envelope.

ACKNOWLEDGEMENTS

LP acknowledges support from the Italian Ministry of Education, University and Research under the FIRB2008 program (RBFR08549F-002) and from the PRIN-INAF 2011 project Multiple Populations in Globular Clusters: Their Role in the Galaxy Assembly. LRY acknowledges support from RFBR grant 14-02-00604 and Presidium of RAS program P-21. The authors acknowledge C Deloye for providing detailed evolutionary tracks for finite entropy WDs. The authors thank an anonymous referee for helpful comments and suggestions.

This research has made use of NASA's Astrophysics Data System.

REFERENCES

Ashok N. M., Banerjee D. P. K., 2003, A&A, 409, 1007
Bildsten L., Townsley D. M., Deloye C. J., Nelemans G., 2006, ApJ, 640, 466
Bildsten L., Shen K. J., Weinberg N. N., Nelemans G., 2007, ApJ, 662, L95
Bours M. C. P., Toonen S., Nelemans G., 2013, A&A, 552, A24
Branch D., Livio M., Yungelson L. R., Boffi F. R., Baron E., 1995, PASP, 107, 1019
Brown W. R., Kilic M., Allende Prieto C., Gianninas A., Kenyon S. J., 2013, ApJ, 769, 66
Carter P. J. et al., 2014, MNRAS, 439, 2848
Cassisi S., Iben I. J., Tornambe A., 1998, ApJ, 496, 376
Chieffi A., Straniero O., 1989, ApJS, 71, 47
Claeys J. S. W., Pols O. R., Izzard R. G., Vink J., Verbunt F. W. M., 2014, A&A, 563, A83
Dan M., Rosswog S., Guillochon J., Ramirez-Ruiz E., 2012, MNRAS, 422, 2417
Dan M., Rosswog S., Brüggen M., Podsiadlowski P., 2014, MNRAS, 438, 14
Deloye C. J., Taam R. E., Winisdoerffer C., Chabrier G., 2007, MNRAS, 381, 525

Drout M. R. et al., 2013, ApJ, 774, 58
Fink M., Hillebrandt W., Röpke F. K., 2007, A&A, 476, 1133
Fink M., Röpke F. K., Hillebrandt W., Seitenzahl I. R., Sim S. A., Kromer M., 2010, A&A, 514, A53
Foley R. J. et al., 2013, ApJ, 767, 57
Fujimoto M. Y., Sugimoto D., 1982, ApJ, 257, 291
García-Senz D., Bravo E., Woosley S. E., 1999, A&A, 349, 177
Goranskij V., Shugarov S., Zharova A., Kroll P., Barsukova E. A., 2010, Perem. Zvezdy, 30, 4
Guillochon J., Dan M., Ramirez-Ruiz E., Rosswog S., 2010, ApJ, 709, L64
Hillebrandt W., Kromer M., Röpke F. K., Ruiter A. J., 2013, Frontiers Phys., 8, 116
Höflich P., Dragulin P., Mitchell J., Penney B., Sadler B., Diamond T., Gerardy C., 2013, Frontiers Phys., 8, 144
Huebner W. F., Merts A. L., Magee N. H., Argo M. F., 1977, Los Alamos Scientific Library Report, LA-6760-M, 1
Iben I., Jr, 1982, ApJ, 259, 244
Iben I., Jr, Tutukov A. V., 1984, ApJS, 54, 335
Iben I., Tutukov A. V., 1985, ApJS, 58, 661
Iben I., Jr, Tutukov A. V., 1989, ApJ, 342, 430
Iben I., Jr, Tutukov A. V., 1991, ApJ, 370, 615
Iben I. J., Tutukov A. V., 1996, ApJS, 105, 145
Idan I., Shaviv N. J., Shaviv G., 2013, MNRAS, 433, 2884 (ISS13)
Iglesias C. A., Rogers F. J., 1996, ApJ, 464, 943
Iijima T., Nakanishi H., 2008, A&A, 482, 865
Kasliwal M. M., 2012, Publ. Astron. Soc. Aust., 29, 482
Kato M., Hachisu I., 1994, ApJ, 437, 802
Kato M., Hachisu I., 2004, ApJ, 613, L129 (KH04)
Kato M., Saio H., Hachisu I., 1989, ApJ, 340, 509
Kato M., Hachisu I., Kiyota S., Saio H., 2008, ApJ, 684, 1366
Kennicutt R. C., Evans N. J., 2012, ARA&A, 50, 531
Kippenhahn R., Weigert A., 1967, Zeitschrift für Astrophysik, 65, 251
Kromer M., Sim S. A., Fink M., Röpke F. K., Seitenzahl I. R., Hillebrandt W., 2010, ApJ, 719, 1067
Kromer M. et al., 2013, ApJ, 778, L18
Limongi M., Tornambè A., 1991, ApJ, 371, 317
Livne E., 1990, ApJ, 354, L53
Livne E., Arnett D., 1995, ApJ, 452, 62
Livne E., Glasner A., 1991, ApJ, 370, 272
Maoz D., Mannucci F., Nelemans G., 2014, ARA&A, 52, 107
Marsh T. R., Nelemans G., Steeghs D., 2004, MNRAS, 350, 113
Mennekens N., Vanbeveren D., De Greve J. P., De Donder E., 2010, A&A, 515, A89
Moll R., Woosley S. E., 2013, ApJ, 774, 137
Moll R., Raskin C., Kasen D., Woosley S. E., 2014, ApJ, 785, 105
Moore K., Townsley D. M., Bildsten L., 2013, ApJ, 776, 97
Nariai K., Nomoto K., Sugimoto D., 1980, PASJ, 32, 473
Nelemans G., Portegies Zwart S. F., Verbunt F., Yungelson L. R., 2001, A&A, 368, 939
Nelemans G., Yungelson L. R., Portegies Zwart S. F., 2004, MNRAS, 349, 181
Nelemans G., Toonen S., Bours M., 2013, in Di Stefano R., Orio M., Moe M., eds, IAU Symp. 281, Binary Paths to Type Ia Supernovae Explosions. Cambridge Univ. Press, Padova, p. 225
Newsham G., Starrfield S., Timmes F., 2013, preprint (arXiv:e-prints)
Nomoto K., 1980, Space Sci. Rev., 27, 563
Nomoto K., 1982a, ApJ, 253, 798
Nomoto K., 1982b, ApJ, 257, 780
Nomoto K., Hashimoto M., 1987, Ap&SS, 131, 395
Nomoto K., Nariai K., Sugimoto D., 1979, PASJ, 31, 287
Paczyński B., 1967, Acta Astron., 17, 287
Paczyński B., 1971, Acta Astron., 21, 1
Pakmor R., Kromer M., Röpke F. K., Sim S. A., Ruiter A. J., Hillebrandt W., 2010, Nature, 463, 61
Pakmor R., Hachinger S., Röpke F. K., Hillebrandt W., 2011, A&A, 528, A117
Pakmor R., Kromer M., Taubenberger S., Sim S. A., Röpke F. K., Hillebrandt W., 2012, ApJ, 747, L10
Pakmor R., Kromer M., Taubenberger S., Springel V., 2013, ApJ, 770, L8
Piersanti L., Cassisi S., Iben I., Jr, Tornambé A., 1999, ApJ, 521, L59
Piersanti L., Cassisi S., Iben I., Jr, Tornambé A., 2000, ApJ, 535, 932
Piersanti L., Cassisi S., Tornambé A., 2001, ApJ, 558, 916
Piersanti L., Gagliardi S., Iben I. J., Tornambé A., 2003, ApJ, 583, 885
Piersanti L., Straniero O., Cristallo S., 2007, A&A, 462, 1051
Piro A. L., Thompson T. A., Kochanek C. S., 2014, MNRAS, 438, 3456
Postnov K. A., Yungelson L. R., 2014, Living Rev. Relativ., 17, 3
Potekhin A. Y., Baiko D. A., Haensel P., Yakovlev D. G., 1999, A&A, 346, 345
Prada Moroni P. G., Straniero O., 2002, ApJ, 581, 585
Raskin C., Scannapieco E., Fryer C., Rockefeller G., Timmes F. X., 2012, ApJ, 746, 62
Rosenbush A. E., 2008, in Werner A., Rauch T., eds, ASP Conf. Ser. Vol. 391, Hydrogen-Deficient Stars. Astron. Soc. Pac., San Francisco, p. 271
Ruiter A. J., Belczynski K., Fryer C., 2009, ApJ, 699, 2026
Ruiter A. J., Belczynski K., Sim S. A., Hillebrandt W., Fryer C. L., Fink M., Kromer M., 2011, MNRAS, 417, 408
Ruiter A. J. et al., 2013, MNRAS, 429, 1425
Saio H., Nomoto K., 1985, A&A, 150, L21
Saio H., Nomoto K., 1998, ApJ, 500, 388
Savonije G. J., de Kool M., van den Heuvel E. P. J., 1986, A&A, 155, 51
Schwab J., Shen K. J., Quataert E., Dan M., Rosswog S., 2012, MNRAS, 427, 190
Shen K. J., Bildsten L., 2007, ApJ, 660, 1444
Shen K. J., Bildsten L., 2009, ApJ, 699, 1365
Shen K. J., Bildsten L., 2014, ApJ, 785, 61
Shen K. J., Kasen D., Weinberg N. N., Bildsten L., Scannapieco E., 2010, ApJ, 715, 767
Sim S. A., Röpke F. K., Hillebrandt W., Kromer M., Pakmor R., Fink M., Ruiter A. J., Seitenzahl I. R., 2010, ApJ, 714, L52
Sim S. A., Fink M., Kromer M., Röpke F. K., Ruiter A. J., Hillebrandt W., 2012, MNRAS, 420, 3003
Solheim J., 2010, PASP, 122, 1133
Solheim J.-E., Yungelson L. R., 2005, in Koester D., Moehler S., eds, ASP Conf. Ser. Vol. 334, 14th European Workshop on White Dwarfs. Astron. Soc. Pac., San Francisco, p. 387
Sparks W. M., Endal A. S., 1980, ApJ, 237, 130
Straniero O., 1988, A&AS, 76, 157
Straniero O., Gallino R., Cristallo S., 2006, Nuclear Phys. A, 777, 311
Straniero O., Cristallo S., Piersanti L., 2014, ApJ, 785, 77
Sugimoto D., Fujimoto M. Y., 1978, PASJ, 30, 467
Taam R. E., 1980a, ApJ, 237, 142
Taam R. E., 1980b, ApJ, 242, 749
Toonen S., Nelemans G., Portegies Zwart S., 2012, A&A, 546, A70
Townsley D. M., Moore K., Bildsten L., 2012, ApJ, 755, 4
Tutukov A. V., Yungelson L. R., 1996, MNRAS, 280, 1035
Uus U., 1970, Nauchnye Informatsii, 17, 25
Waldman R., Sauer D., Livne E., Perets H., Glasner A., Mazzali P., Truran J. W., Gal-Yam A., 2011, ApJ, 738, 21
Wang B., Meng X., Chen X., Han Z., 2009, MNRAS, 395, 847
Wang B., Justham S., Han Z., 2013, A&A, 559, A94
Webbink R. F., 1984, ApJ, 277, 355
Wolf W. M., Bildsten L., Brooks J., Paxton B., 2013, ApJ, 777, 136
Woosley S. E., Kasen D., 2011, ApJ, 734, 38
Woosley S. E., Weaver T. A., 1994, ApJ, 423, 371
Woosley S. E., Taam R. E., Weaver T. A., 1986, ApJ, 301, 601
Woudt P. A., Steeghs D., 2005, in Hameury J.-M., Lasota J.-P., eds, ASP Conf. Ser. Vol. 334, The Astrophysics of Cataclysmic Variables and Related Objects. Astron. Soc. Pac., San Francisco, p. 451
Woudt P. A. et al., 2009, ApJ, 706, 738
Yoon S.-C., Langer N., 2003, A&A, 412, L53
Yoon S.-C., Langer N., 2004, A&A, 419, 645
Yungelson L. R., 2008, Astron. Lett., 34, 620

Table A1. From left to right we report the values of A and the corresponding standard deviation, the values of B and the corresponding standard deviation, in equation (A1), as well as the correlation coefficient R^2. RG/SS represents the transition line between the RG and the steady accretion regimes; SS/MF the transition line between the steady accretion and the mild flashes regimes; MF/SF the transition line between the mild flashes and the strong flashes regimes; SF/Dt the transition line between the strong and dynamical flashes regimes.

	A	σ_A^2	B	σ_B^2	R^2
RG/SS	−6.840	0.026	1.349	0.029	0.999
SS/MF	−8.115	0.151	2.290	0.170	0.986
MF/SF	−8.233	0.029	2.022	0.042	0.999
SF/Dt	−8.313	0.026	1.018	0.037	0.997

APPENDIX A: INTERPOLATION FORMULAE

In this appendix we provide interpolation formulae for the data reported in the manuscript, which could be directly used in population synthesis codes to describe the evolution of WDs accreting He-rich matter.

A1 Accretion regimes

The values of $\dot{M}$ as a function of the WD initial mass at which the transition from one accretion regime to another occurs (see Fig. 2) is given by:

$$\log(\dot{M}) = A + B M_{\rm WD}, \tag{A1}$$

where $\dot{M}$ is expressed in $\mathrm{M}_\odot\ \mathrm{yr}^{-1}$ and $M_{\rm WD}$ in $\mathrm{M}_\odot$. In Table A1, we report the values of the coefficients A and B for the various accretion regimes. These fits are valid for WDs with initial masses in the range 0.596 78–1.019 48 $\mathrm{M}_\odot$.

A2 Dynamical flashes regime

For a fixed value of the initial WD mass, for models experiencing a dynamical He flash as a result of direct accretion of He-rich matter, the mass accreted before the onset of the dynamical flash ($\Delta M_{\rm He}$) can be expressed as a function of $\dot{M}$ by the following relation:

$$\Delta M_{\rm He} = \sum_{i=0}^{4} F_i \times \dot{M}^i, \tag{A2}$$

where $\Delta M_{\rm He}$ is in $\mathrm{M}_\odot$ and $\dot{M}$ in $10^{-8}\ \mathrm{M}_\odot\ \mathrm{yr}^{-1}$. In Table A2 we report the values of the coefficients in equation (A2) for the five initial WD models considered in the present work (see Table 1).

A3 Strong flashes regime

For a fixed value of the mass of an accreting WD, the accumulation efficiency ($\eta_{\rm acc}$) as a function of $\dot{M}$ for the models experiencing the first strong non-dynamical He flash is provided by the following relation:

$$\eta_{\rm acc} = \sum_{i=0}^{3} G_i \times \dot{M}^i, \tag{A3}$$

where $\dot{M}$ is expressed in $10^{-8}\ \mathrm{M}_\odot\ \mathrm{yr}^{-1}$. In Table A3, we report the values of the coefficients for the five initial WD models considered in the present work (see Table 1).

Table A2. For each initial WD model, we report the values of the F_i coefficients and the corresponding standard deviation $\sigma_{F_i}^2$ in equation (A2). We also report the value of the correlation coefficient R^2, as well as the range of validity of the fits ($\dot{M}_{\rm min} - \dot{M}_{\rm max}$ in $10^{-8}\ \mathrm{M}_\odot\ \mathrm{yr}^{-1}$).

	M060	M070	M081
F_0	0.718 ± 0.012	0.625 ± 0.012	0.528 ± 0.008
F_1	−0.762 ± 0.067	−0.671 ± 0.062	−0.623 ± 0.047
F_2	0.744 ± 0.101	0.598 ± 0.082	0.665 ± 0.078
F_3	−0.259 ± 0.042	−0.183 ± 0.027	−0.324 ± 0.045
F_4	–	–	0.052 ± 0.008
R^2	0.996	0.994	0.998
$\dot{M}_{\rm min} - \dot{M}_{\rm max}$	0.1 – 1.5	0.1 – 2.0	0.15 – 2.5
	M092	M102	
F_0	0.440 ± 0.007	0.319 ± 0.009	
F_1	−0.489 ± 0.035	−0.240 ± 0.030	
F_2	0.452 ± 0.052	0.105 ± 0.027	
F_3	−0.198 ± 0.026	−0.024 ± 0.009	
F_4	0.029 ± 0.004	0.0021 ± 0.0009	
R^2	0.998	0.989	
$\dot{M}_{\rm min} - \dot{M}_{\rm max}$	0.15 – 3.0	0.15 – 5.0	

Table A3. For each initial WD model, we report the values of the G_i coefficients and the corresponding standard deviation $\sigma_{G_i}^2$ in equation (A3). We also report the value of the correlation coefficient R^2, as well as the range of validity of the fits ($\dot{M}_{\rm min} - \dot{M}_{\rm max}$ in $10^{-8}\ \mathrm{M}_\odot\ \mathrm{yr}^{-1}$).

	M060	M070
G_0	0.006 ± 0.121	−0.035 ± 0.030
G_1	0.051 ± 0.070	0.075 ± 0.012
G_2	0.0083 ± 0.0121	−0.0018 ± 0.0014
G_3	$(-3.317 \pm 6.4) \times 10^{-4}$	$(3.266 \pm 4.2) \times 10^{-5}$
R^2	0.996	0.999
$\dot{M}_{\rm min} - \dot{M}_{\rm max}$	2.5 − 10	3 − 20
	M081	M092
G_0	0.093 ± 0.021	−0.0759 ± 0.026
G_1	0.018 ± 0.005	0.0154 ± 0.004
G_2	0.0016 ± 0.0004	0.0004 ± 0.0002
G_3	$(-4.111 \pm 0.73) \times 10^{-5}$	$(-5.905 \pm 1.56) \times 10^{-6}$
R^2	0.999	0.998
$\dot{M}_{\rm min} - \dot{M}_{\rm max}$	4 − 30	5 − 60
	M102	
G_0	−0.323 ± 0.017	
G_1	0.041 ± 0.002	
G_2	−0.0007 ± 0.000 06	
G_3	$(4.733 \pm 0.55) \times 10^{-6}$	
R^2	0.999	
$\dot{M}_{\rm min} - \dot{M}_{\rm max}$	8 − 70	

SUPPORTING INFORMATION

Additional Supporting Information may be found in the online version of this article:

(http://mnras.oxfordjournals.org/lookup/suppl/doi:10.1093/mnras/stu1885/-/DC1).

Please note: Oxford University Press is not responsible for the content or functionality of any supporting materials supplied by the authors. Any queries (other than missing material) should be directed to the corresponding author for the article.

This paper has been typeset from a TEX/LATEX file prepared by the author.